Green Synthesis of Copper Oxide with MgAl Layered Double Hydroxide Nanocomposite for Degradation of Methylene Blue

Hildana Tesfaye Berede

A thesis Submitted to

The Department of Materials Science and Engineering

School of Mechanical, Chemical and Materials Engineering

Presented in Partial Fulfillment of the Requirement for the Degree of Master's in Materials science and engineering

Office of Graduate Studies

Adama Science and Technology University

June, 2022

Adama, Ethiopia

Green Synthesis of Copper Oxide with MgAl Layered Double Hydroxide Nanocomposite for Degradation of Methylene Blue

Hildana Tesfaye Berede

Advisor: Osman Ahmed (Ph.D.)

Co-advisor: Dinsefa Mensur (Ph.D.)

A thesis Submitted to

The Department of Materials Science and Engineering

School of Mechanical, Chemical and Materials Engineering

Office of Graduate Studies

Adama Science and Technology University

June, 2022

Adama, Ethiopia

Declaration

I hereby declare that this Master Thesis entitled "**Green Synthesis of Copper Oxide with MgAl Layered Double Hydroxide Nanocomposite for Degradation of Methylene Blue**" is my original work. That is, it has not been submitted for the award of any academic degree, diploma or certificate in any other university. All sources of materials that are used for this thesis have been duly acknowledged through citation.

Hildana Tesfaye	_____	_____
Name of student	Signature	Date

Recommendation of Advisors/ Supervisors

I/we, the advisor (s) of this thesis, hereby certify that I/we have read the revised version of the thesis "**Green Synthesis of Copper Oxide with MgAl Layered Double Hydroxide Nanocomposite for Degradation of Methylene Blue**" prepared under my/our guidance by Hildana Tesfaye Submitted in partial fulfillment of the requirements for the degree of Mater's of Science in Materials science and engineering. Therefore, I/we recommend the submission of revised version of the thesis to the department following the applicable procedures.

_____	_____	_____
Major Advisor/Supervisor	Signature	Date
_____	_____	_____
Co-advisor/Co-supervisor	Signature	Date

Approval Sheet

I/we, the advisors of the thesis entitled "**Green Synthesis of Copper Oxide with MgAl Layered Double Hydroxide Nanocomposite for Degradation of Methylene Blue**" and developed by Hildana Tesfaye; hereby certify that the recommendation and suggestions made by the board of examiners are appropriately incorporated into the final version of the thesis.

Major Advisor	Signature	Date
Co-Advisor	Signature	Date

We, the undersigned, members of the Board of Examiners of the thesis by Hildana Tesfaye have read and evaluated the thesis entitled "**Green Synthesis of Copper Oxide with MgAl Layered Double Hydroxide Nanocomposite for Degradation of Methylene Blue**" and examined the candidate during open defense. This is, therefore, to certify that the thesis is accepted for partial fulfillment of the requirement of the degree of Master of Science in Materials Science and Engineering.

Chairperson	Signature	Date
Internal Examiner	Signature	Date
External Examiner	Signature	Date

Finally, approval and acceptance of the thesis is contingent upon submission of its final copy to the Office of Postgraduate Studies (OPGS) through the Department Graduate Council (DGC) and School Graduate Committee (SGC).

Department Head	Signature	Date
School Dean	Signature	Date
Office of Postgraduate Studies, Dean	Signature	Date

ACKNOWLEDGEMENTS

First and foremost, I would want to praise and thank God, the Almighty, who has blessed the writer with numerous blessings, knowledge, and opportunities, allowing me to finally complete the thesis.

After that, my sincerest gratitude and respect go to my advisor Osman Ahmed (Assoc Prof.) for his unconditional support, patience, inspiration, vast knowledge, and advice that aided me throughout the research and writing of this thesis.

Besides, I would like to extend my sincere thanks to my co-advisor, Dinsefa Mensur (Assoc Prof.), for his time, advice, and encouragement.

I would like to give special thanks to all of my colleagues, and Materials Science and Engineering staff members, for overcoming a significant challenge. We had completed all of the laboratory research and some of the necessary characterizations processes here with the help of Mr. Demeke Tesfaye. I would also express my deep sense of gratitude to the Department of Materials Science and Engineering at National Taiwan University of Science and Technology.

Finally, no one has been more crucial to me in the completion of this endeavor than my family members. I would like to thank my parents for always supporting and guiding me.

TABLE OF CONTENTS

LIST OF TABLES

LIST OF FIGURES

LIST OF ACRONYMS

XRD	X-Ray Diffraction
UV-Vis DRS	Ultra Violet-Visible Diffuse Reflectance Spectroscopy
FTIR	Fourier Transform Infrared Spectroscopy
TEM	Transmission Electron Microscopy
XPS	X-ray Photoelectron Spectroscopy
SEM	Scanning Electron Microscopy
PL	Photoluminescence Spectroscopy
MB	Methylene Blue
CuO	Copper Oxide
LDH	Layered Double Hydroxide
NPs	Nanoparticles
OP	Onion Peel
ROS	Reactive Oxygen Species
AOP	Advanced Oxidation Process
MNPs	Metal Nanoparticles
CLDHs	Calcined Layered Double Hydroxides

ABSTRACT

Photocatalysis is one of the most promising and cost-effective technologies to eliminate organic pollutants. Copper (II) oxide nanoparticles are well-known photocatalysts for degrading organic pollutants due to its natural abundance, low cost, low toxicity, and high catalytic activity. This study used Allium cepa L. peels extract to synthesized copper oxide nanoparticles, which were then immobilized on the surface of MgAl-layered double hydroxide to form CuO/MgAl-LDH nanocomposites with different weight ratio of CuO/LDH (1:1, 1:2, and 2:1) via co-precipitation method. Various characterization techniques were used to characterize all synthesized nanocomposites. The degradation of cationic methylene blue (MB) under visible light irradiation was used to assess the photocatalytic performance of the synthesized catalysts. All of the as-synthesized nanocomposites were effective photocatalysts for the photodegradation of an MB solution; however, the CuO/MgAl-LDH (1:2) had the best photocatalytic ability of the catalysts studied, achieving 99.20 % MB degradation in 80 minutes under visible-light irradiation. The photocatalytic activity of the nanocomposites was significantly greater than that of pristine CuO NPs made in the same way, due to their uniform distribution of CuO NPs, which facilitates the generation of electrons and holes pairs, improves charge transfer, and reduces charge recombination. By providing enough space for NPs distribution, the LDH was able to induce the required photostability. The CuO/MgAl-LDH (1:2) nanocomposites exhibited a pseudo-first-order rate constant reaching a maximum value of 0.03141min^{-1}. CuO/MgAl-LDH (1:2) nanocomposites can be easily regenerated and reused for up to five cycles without any significant loss of the catalytic activity. In addition, a possible methylene blue degradation mechanism was proposed.

Keywords: *Allium cepa L., layered double hydroxide, cupric oxide, Nanocomposite, photocatalysis, methylene blue*

CHAPTER-ONE

1. INTRODUCTION

1.1. Background of the Study

Water is the most abundant natural resource on the planet, accounting for 75 % of all water in the crust. It is an important component of the aquatic living system as well as human drinking, whether for home, industrial, agricultural, or other purposes (Sathiyavimal et al., 2021). Environmental pollution problems have been seriously increased throughout the world due to the development of industrialization and modernization. Domestic wastewater and industrial/ commercial wastewater are the two major types of water pollutants that are defined and based mainly on their origin. Organic and inorganic contaminants, as well as microorganisms, are immediately dumped into the environment, contaminating wastewater (Mousa, 2013; Zheng, Cheng, You, Yu, & Ho, 2019). Textile, plastic, paper, leather, and other industries (Li et al., 2017; Sun et al., 2019; Zelekew & Kuo, 2017) produce toxic and hazardous effluents into the environment, which have significant effects for the environment and human health because of their carcinogenic and mutagenic properties (Daud et al., 2019). The most often used insecticides, textiles, medicines, fungicides, and other manufacturing businesses employ organic pollutants such as nitrophenol, methylene blue, methyl orange, methyl green, Congo red, and others. They are released into bodies of water, posing a threat to aquatic life and human health (Manjari, Saran, Arun, Rao, & Devipriya, 2017). Among organic dyes, methylene blue (MB) is one of the most commonly used dye materials in wood, silk, and cotton. In veterinary medicine as well as for diagnostic and therapeutic purposes in humans, the same dye is used. Eye burns are sometimes permanent after exposure to MB. As a result of inhaling MB, a person feels difficulty breathing, sweats profusely, has a burning sensation in the mouth, their heartbeat increases rapidly, sweats excessively, vomits, and experiences headaches (Muthuvel, Jothibas, & Manoharan, 2020). As a result, attention should be paid when treating MB in aqueous solution.

The photocatalytic dye degradation utilizing semiconductors was proven to be an effective technique for purifying wastewater containing persistent dyes under solar irradiation (Kumari, Kaushal, & Singh, 2022). The visible light-assisted heterogeneous photocatalysis approach generates clean energy without producing secondary pollutants during the

mineralization of environmental contaminants, and economically viable. The superoxide and hydroxyl radicals produced during photocatalysis are highly reactive, mineralizing contaminants near the photocatalysts' surface (Rao, Sathishkumar, et al., 2018). Various photocatalysts such as TiO_2 (Varnagiris et al., 2020), ZnO (Sanakousar, Vidyasagar, Jiménez-Pérez, & Prakash, 2022), Fe_2O_3 (Abhilash, Akshatha, & Srikantaswamy, 2019) and CuO (Alsamhary, Al-Enazi, Alhomaidi, & Alwakeel, 2022) have been investigated.

CuO NPs are a good choice for purifying water and removing industrial effluents from the environment during advanced oxidation processes (AOPs), due to its excellent photovoltaic properties, robust electro conductivity, and low band gap (Gu, Chen, Chen, Zhou, & Parsaee, 2018; Hossain et al., 2020). As a result, it's commonly utilized as a photocatalyst in a wide range of processes (Rao, Wu, Asiri, Anandan, & Ashokkumar, 2018). Several physical and chemical methods are being used to synthesis CuO NPs, but these methods have several problems like high temperature and pressure, requires reducing agent, organic solvents and hazardous chemicals (Bordbar, Sharifi-Zarchi, & Khodadadi, 2017). To resolve these problems, an inexpensive, environmental-friendly, simple and non-toxic biological route is applied to fabricate CuO NPs. In addition, using plant and plant extracts are considered as potential candidate due to its simplicity, large scale production and easy handling owing to natural reducing and capping agents when compared to microorganisms (M. Rafique et al., 2020). Several studies have reported the application of CuO NPs in an aqueous medium for photocatalytic degradation of organic contaminants, such as *Solanum lycopersicum* (Vaidehi, Bhuvaneshwari, Bharathi, & Sheetal, 2018), *Citrofortunella microcarpa* (M. Rafique et al., 2020), *Solanum nigrum* (Muthuvel, Jothibas, & Manoharan, 2020), *Psidium guajava* (Sathiyavimal et al., 2021) and so on. The biosynthesis of CuO NPs using the peel extract of *Allium cepa L*. has not yet been reported. Onion (Allium cepa) is a vegetable harvested worldwide for its pharmaceutical, nutritional, and other functional properties. However, its peel is usually thrown away as organic waste and it can be treated and managed in environmental treatment facilities. Moreover, the peel contains high concentrations of flavonoids and polyphenol compounds, acting as reducing and capping agents for nanoparticles (Chia, Lim, Tan, Yong, & Kan, 2019; Lem, Yoon, Bae, & Lee, 2021).

Nonetheless, CuO's photocatalytic activity is limited due to its high e^-/h^+ recombination rate and limited charge collection is the considerable discrepancy between carrier diffusion length and optical absorption depth (Dasineh Khiavi et al., 2019). To improve the stability of photogenerated electron and hole pairs, many strategies were used, including making specialized structures (A. George et al., 2022), doping (Islam, Saiduzzaman, Nishat, Kabir, & Farhad, 2021), heterojunction with appropriate conduction and valence band locations (Hossain et al., 2020; Senobari & Nezamzadeh-Ejhieh, 2018; J. Zhang et al., 2019), or loading on various supports (Soori & Nezamzadeh-Ejhieh, 2018). Supported catalysts have a higher decomposition rate than unsupported catalysts, which can be attributed to greater organic substrate condensation on the supported catalyst via adsorption and a reduction in electron-hole recombination on the surface (Khan, Khan, Usman, Imran, & Saeed, 2020). Researchers reported using a variety of support medium to slow the aggregation of NPs, including zeolite (Soori & Nezamzadeh-Ejhieh, 2018), Graphene oxide (Ganesan et al., 2020), carbon nanotubes (Sapkota et al., 2020), nanoclay (Khan et al., 2020), layered double hydroxides (Le Hoang, Insin, & Sukpirom, 2020), and so on.

Layered double hydroxides have been known as hydrotalcite-like compounds. They are inorganic layered substances made up of positively charged brucite-like host layers and charge-balancing interlayer anions, and their large surface areas make them ideal catalysts or precursors (Ma et al., 2015). Layered double hydroxides (LDHs) are commonly employed in catalysis, adsorption, electrochemistry, and biotechnology as typical two dimensional-nano structured anionic clays (Zhao et al., 2018). Apart from the multiple positive charges on the LDHs platelets, the heterojunction interface has enough of interlayer water molecules and hydroxide ions to form HO•. The layer structure, in particular, may improve the effectiveness of photocatalytic processes by encouraging electron transport, inhibiting electron and hole recombination rate, and preventing nanoparticle aggregation (L. Wang et al., 2019). Because of their superior properties, LDHs was deemed an appropriate substrate for growing various nanoparticles to achieve synergistic effects and improved properties. As photocatalyst support, binary layered double hydroxides with magnesium and aluminum in the laminate have been widely used (X. Li et al., 2019; Ma et al., 2015; Zheng et al., 2019).

MgAl-LDH, in particular, is the most representative of several types of hydrotalcite. Under visible light irradiation, however, MgAl-LDH alone has very limited photocatalytic activity. Fortunately, LDHs' layered structure has been shown to be beneficial for electron migration and electron-hole pair recombination suppression; Furthermore, the large number of hydroxyl groups on LDH laminates can generate more highly active •OH species, which is useful for boosting the photocatalytic reaction's quantum efficiency (Y. Wang et al., 2018). For diverse photocatalytic applications, a range of semiconductor and MgAl-LDH composites, such as TiO_2/MgAl-LDH (Seftel, Mertens, & Cool, 2013), SnO_2/MgAl-LDH (Dvininov, Ignat, Barvinschi, Smithers, & Popovici, 2010), CeO_2/MgAl-LDH (Valente, Tzompantzi, & Prince, 2011), $AgSiO_x$/MgAl-LDH (Y. Wang et al., 2018), and TiO_2@MgAl-LDH (L. Wang et al., 2019) have been described. In addition, MgAl-LDH is a wide bandgap semiconductor material that can be employed as a monomer to create a heterojunction structure (P. Chen et al., 2020). To our knowledge, this is the first time a green approach using *Allium cepa L*. peel extract has been applied for the synthesis of CuO NPs supported by MgAl-LDH.

In the present work, our main goal is to improve the photocatalytic efficiency of CuO NPs by using layered double hydroxides (MgAl-LDHs) as a matrix to incorporate CuO NPs within. To evaluate the degradation activity of CuO/MgAl layered double hydroxides composite under visible light irradiation, methylene blue was used as a model organic pollutant. CuO/MgAl-LDH composites with various CuO/LDH weight ratios were made, and their catalytic capabilities were compared to phase of pure CuO and LDH particles. The possibility of a photocatalytic degradation mechanism of methylene blue by the composite was also proposed. It is expected that the composite catalysts could have improved performance than the single components due to uniform dispersion of CuO NPs, and high adsorption capacity of LDH.

1.2. Statement of Problems

Rapid development of population, agricultural and industrial activities are leading to exponential increase in release of hazardous pollutants such as synthetic dye-stuff, benzene, hydrocarbons, sulphonamides, polychlorinated biphenyls (PCBs), phthalates, aromatic nitro compounds, phenols etc., (Filiz, 2020). Methylene blue (MB), for example, is a poisonous, non-biodegradable chemical commonly used in the textile industry (Sakib et al., 2019).

However, with the suitable catalyst, it can be decomposed into CO_2, H_2O, or inorganic ions. Visible-light-driven photocatalysis in an appropriate photocatalyst has proven to be an efficient and environmentally benign way among numerous. Metal oxide semiconductors have recently attracted a lot of attention because of their unusual physical and chemical properties, such as optical, catalytic, and magnetic capabilities. Cupric oxide NPs have risen to prominence among photocatalysts in the remediation of environmental contaminants, and it possesses several distinguishing characteristics that make them an ideal photocatalytic system, including being less expensive, safe, efficient, easy to use, photo-stable, and having a high photocatalytic performance across the solar spectrum (Ganesan et al., 2020). CuO NPs, on the other hand, are unstable and easily self-aggregate due to their large surface area and high surface energy (Z. Zhou, Lu, Wu, & Zhang, 2013). Despite this, the photocatalytic efficiency of copper oxide remains low due to the extremely fast recombination rate of the photogenerated electron-hole pairs (Choi et al., 2017). To circumvent these drawbacks, a range of less expensive and high surface area supporting materials have been effectively employed to prevent aggregation, inhibit recombination rate by bringing organic pollutant molecules near the catalyst surface due to their high adsorption capacity, and thus increase the decomposition rate of CuO NPs. Combining LDHs' strong adsorptive capacity with CuO NPs' high catalytic activity for organic pollutant degradation should offer promising results.

1.3. General Objective

- To synthesize and characterize of bio-assisted CuO NPs with MgAl-LDHs nanocomposite for organic pollutant remediation in wastewater.

1.4. Specific Objectives

- Synthesize cupric oxide nanoparticles using *Allium cepa L*. peels extract as reducing and capping agent.
- To prepare MgAl LDHs by using co-precipitation method.
- To synthesize the nanocomposites of layered double hydroxides and CuO.
- To characterize the synthesized CuO/MgAl-LDHs nanocomposite using different characterization techniques.
- To test the photocatalytic performance of the prepared catalysts.

1.5. Significance of the Study

Water pollution caused by organic and inorganic impurities has a harmful influence on the environment and individuals because of its carcinogenic and mutagenic properties. Because of their low cost, non-toxicity, and wide availability, metal oxide NPs have gotten a lot of attention for a variety of applications. Despite their prominence, they are insecure. As a result, immobilizing them on large-surface-area LDHs can improve their catalytic efficiency. We synthesized and tested CuO NPs/MgAl-LDHs nanocomposites for photocatalytic activity against methylene blue in wastewater. The use of discarded bio-waste from onion peels in the manufacture of nanoparticles not only solves the problem of disposal, but it also has the potential to operate as a reducing and capping agent. The amount of onion peel trash dumped directly into the environment would be minimized, and clean water availability would be increased.

1.6. Scope of the Study

In this work, CuO NPs/MgAl-LDHs nanocomposites has been fabricated through co-precipitation processing using onion peel extract as reducing and stabilizing agent. Materials characterizations were followed by the evaluation of as-synthesized nanostructure for the degradation of organic pollutants under visible light. The mechanism of reaction was also proposed.

CHAPTER-TWO

2. LITERATURE REVIEW

2.1. Water Pollution

Pollution occurs when toxins are introduced into the natural environment and produce negative consequences. Foreign substances/energies or naturally occurring pollutants both contribute to pollution. Vital forms of pollution include air, light, soil, litter, noise, visual, plastic, radioactive, thermal, and water pollution (Asano & Levine, 1996). Water pollution (or aquatic pollution) is the contamination of water bodies, usually resulting when contaminants are introduced into the natural environment by human activities. For example, discharging inadequately treated wastewater into water bodies can lead to the degradation of aquatic ecosystems. As a result, people living downstream may face public health concerns. They may use the same polluted river water for drinking, bathing, or irrigation. Water pollution is the leading worldwide cause of death and disease, for example, water-borne diseases (Rijsberman, 2006).

Water bodies have been polluted by inorganic (Zubair, Daud, McKay, Shehzad, & Al-Harthi, 2017) and organic (Kumar, Mohapatra, Dharmadhikari, & Ghosh, 2020) contaminants. The contaminants are industrial effluents, detergents, bacteria, Plant debris, and unsafe sewage disposals are commonly happening (Y. Zhang et al., 2016). Due to the increasing demand for clean and safe water for such purposes as drinking, industrial, and irrigation, it is necessary to consider the best ways to purify wastewater for reuse purposes (Y.-g. Wu, Wen, Wu, & Fang, 2014). Numerous treatment techniques such as Coagulation, filtration (Zhi, Li, Zhang, & Wang, 2010), evaporation, distillation, and adsorption (Sobhana, Sarakha, Prevot, & Fardim, 2016) and others have been attempted to mitigate pollutants (Madima, Mishra, Inamuddin, & Mishra, 2020; Shan et al., 2014). Although they are ineffective since they transfer pollution from one form to another (Bilal Tahir, Nadeem Riaz, & Asiri, 2019).

2.2. Metal Oxide Semiconductors

Organic dyes are often degraded and mineralized into less hazardous chemicals such as CO_2, H_2O, and inorganic ions via the production of highly reactive oxygen species (ROS) such as $\bullet O_2^-$, $\bullet OH$, or $HO_2\bullet$ radicals and subsequent oxidation of organic compounds in advanced

oxidation process (AOP). The heterogeneous photocatalytic process, in particular, is the most successful approach in all known AOPs due to its high availability, low toxicity, low costs, and diversified nature, which may tackle a wide range of water contaminants. This method, also known as photocatalysis, uses semiconductor catalysts to generate reactive oxygen species (ROS) and break down organic pollutants, making it a powerful approach for extracting colors and other organic compounds from wastewater (Lim & Ho, 2017).

The most commonly investigated photocatalysts for various purposes are TiO_2 and ZnO. Both photocatalysts, however, have the following drawbacks: their ability to absorb visible light is minimal, and they aggregate quickly during heterogeneous photocatalysis. To avoid such limitations, researchers have made several changes to improve the effectiveness of the photocatalysts that result. Among the modifications in heterogeneous photocatalysis, p-n heterojunction photocatalysts have gotten a lot of interest because of their improved efficiency in pollutant degradation. However, the aggregation of heterojunction photocatalysts prohibits permanent usage (Rao, Sathishkumar, et al., 2018). Due to the high cost of producing UV radiation, these materials are not as effective as they could be. Furthermore, because the spectrum distribution of solar energy contains ~45 % visible light and just 5% UV radiation, extensive photocatalysis applications are viable if the catalysis technique can be performed under readily available, cost-effective visible light (Islam et al., 2021).

2.3. Copper Oxide (CuO)

Copper (II) oxide nanoparticles (CuO NPs), p-type metal oxide semiconductor belonging to the monoclinic structure with a narrow band gap energy (E_g) 1.2 eV-1.9 eV (Bhaduri & Kajal, 2019), are cheap, abundant and economic material. CuO is an indirect bandgap semiconductor with a carrier diffusion length of roughly 200 nm, and an optical absorption depth of around 500 nm (Masudy-Panah, Zhuk, Tan, Gong, & Dalapati, 2018). CuO NPs can be used for antimicrobial and antiviral effects, superconductors, gas sensors, biosensors, super capacitors, nano fluids, solar cells, lithium batteries, pollution remediation and so on, due to the properties of high surface-to-volume ratio that makes them very reactive, good catalytic activity, high optical transparency, fair stability, cost-effectiveness and readily available compared to other expensive noble metals like Au, Pt, and Ag (Buazar, Sweidi, Badri, & Kroushawi, 2019; Chowdhury, Khan, & Rashid, 2020; Keabadile, Aremu, Elugoke, &

Fayemi, 2020; Manjari, Saran, Arun, Rao, & Devipriya, 2017). Copper oxide nanoparticles are suitable for purifying water and removing industrial effluents from the environment, such as, pathogens (Mousa, 2013), organic dyes (Das, Ghosh, Ghosh, Dam, & Baskey, 2018; M. Rafique et al., 2020), nitrophenol (Buazar et al., 2019) and so on. For instance, Mandlimath *et al*. reported that CuO, Co_3O_4, Fe_2O_3, and NiO all helped to accelerate the reduction process. At room temperature (30 °C), oxides such TiO_2, V_2O_5, Cr_2O_3, MnO_2, and ZnO were found to be inactive in the conversion of nitrophenol using aqueous sodium borohydride (Mandlimath & Gopal, 2011). The chemical and physical properties of nanomaterials are largely determined by their shape, size, and microstructures, as is well known. As a result, depending on the experimental conditions, these can be modified (Goel, Chen, & Cai, 2014). While various physical and chemical methods for synthesizing metal oxide nanostructures have been discovered, the production of this important category of nanostructures has drawbacks such as expensive reagent, hazardous reaction conditions, longer time, and a time-consuming process to isolate nanoparticles (Das et al., 2018; Lucchesi Schio, Farias Soares, Machado, & Barcellos, 2021). As a result, there is potential to create novel methods for the synthesis of nanoparticles that require an inexpensive reagents, less harsh reaction conditions, and are environmentally friendly, which is called green approach (Asemani & Anarjan, 2019).

2.3.1. Synthesis of CuO NPs using Plant Extract

2.3.1.1. Preparation of Plant Extract

Plant extract is made by dissolving plant parts (leaves, peels, seeds, flowers, roots and so on) in a solvent such as distilled water (M. Rafique et al., 2018), ethanol or methanol (Rani Verma & Khan, 2019), and boiling, then cooling at room temperature, centrifugation, and filtration. Finally, the filtrates are kept at 4-10 ℃ for further experiments.

2.3.1.2. Synthesis of CuO NPs

Copper oxide nanoparticles are successfully synthesized using plant extract as reducing and stabilizing agents. Initially, 4.0 g copper acetate monohydrate was dissolved in 10 mL deionized water and stirred for 10 minutes at room temperature with a magnetic stirrer. After that, 30 mL P. guajava leaf extract (pH 7.5) was added drop by drop to the 10 mL copper acetate monohydrate at 60 °C for 4 hours with continuous stirring (250 rpm). The solution

turned blackish jelly after adding the leaf extract, and it was heated for another 30 minutes to evaporate any leftover water. The sample was then calcined in a furnace at 400 °C for 4 hours, resulting in black CuO NPs. The following is a description of a proposed CuO NPs synthesis mechanism (Singh, Kumar, Kim, & Rawat, 2019):

$$Cu(CH_3COO)_2 + \text{plant extract} \rightarrow Cu(OH)_2 \quad (1)$$

$$Cu(OH)_2 + \text{calcination} \rightarrow CuO + H_2O \quad (2)$$

In a 100 mL beaker, 40 mL of the cupric solution was placed, and 40 mL of freshly made seed extract was added dropwise for copper ion reduction, followed by the addition of 200 mL of ammonia solution while constantly stirring. Over the course of 5 hours, the blue-colored solution turned green, and at around 7 hours, a dark brown precipitate appeared. The appearance of the brown precipitate indicated that copper ions had been completely reduced and CuO NPs had formed. The resulting solution was centrifuged and rinsed many times with deionized water before being heated for an hour at 450 °C (Sukumar, Rudrasenan, & Padmanabhan Nambiar, 2020).

CuO NPs were produced by adding 1.2 g $Cu(NO_3)_2.3H_2O$ in 100 mL double distilled water to two round bottom flasks containing 10 mL each of flower extract (FE) and seed extract (SE). Then, to achieve pH 10, 5 mL of liquid NH_3 solution was added and quickly stirred to ensure thorough mixing. When heated at 55 ^oC for 4 hours, the color of the mixture changed from blue to blackish green. The product was collected, washed, and dried in a 70 °C oven in the case of SE. However, in the case of FE, once the heating process was completed, the material was refluxed at 110 ^oC for 8 hours before being filtered, washed, and dried in an oven at the same temperature. After that, both samples were annealed for 5 hours at 200 °C (Das et al., 2018).

1 mL of *Murayya koenigii* leaf extract was added to 10 mL of 5 mM aqueous copper (II) sulphate, $CuSO_4$, and the pH of the mixture was adjusted to pH 11 using 0.1 M sodium hydroxide, NaOH solution for the production of CuO NPs. The reaction mixture was agitated, and the color progressively changed from light brown to dark brown, indicating the creation of CuO NPs. The colloidal particles were centrifuged for 20 minutes at 14800 rpm, and the resulting precipitate was rinsed with deionized water before being dried in the desiccator for

further use. The schematic diagram of a CuO NP biosynthesis and stabilization mechanism is shown in Fig.1 (Nordin & Shamsuddin, 2019).

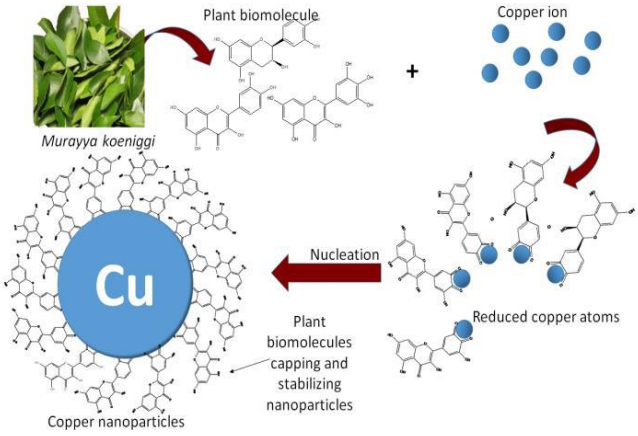

Fig. 1. Proposed mechanism for the formation and stabilization of CuO NPs (Nordin & Shamsuddin, 2019).

2.3.2. Removal of Pollutants by CuO Nanomaterial's

2.3.2.1. Removal of Phenols and its Derivatives

4-Nitrophenol (4-NP) is a hazardous substance that affects humans and animals' livers, kidneys, and central nervous systems (Ghorai, 2015). The Environmental Protection Agency (EPA) has designated 4-NP as a priority pollutant (Yang et al., 2018). Plant extract mediated CuO NPs were used to study the catalytic conversion of 4-nitrophenol to 4-aminophenol. Nasrollahzadeh *et al*. devised a green synthesis technique for CuO nanoparticles using *Gundelia tournefortii* aqueous extract as a mild, renewable, and non-toxic reducing agent. More notably, the greenly produced CuO NPs showed high catalytic activity for the reduction of 4-nitrophenol. The catalyst was easily separated, and the recovered catalyst could be reused multiple times without losing its catalytic activity (Nasrollahzadeh, Maham, & Sajadi, 2015). Thirumarimurugan *et al*. focused on facile and eco-friendly fabrication of copper oxide nanoparticles (CuO NPs) using *Tecoma castanifolia* leaf extract. The obtained NPs were found roughly spherical in shape with size less than 100 nm. Phytofabricated CuO NPs exhibits efficient catalytic reduction of 4-nitrophenol (4-NP) to 4-aminophenol (4-AP) within 14 minutes and reaction follows pseudo-first-order kinetics with the apparent rate constant (K_{app})

of 0.18 min^{-1} (Sharmila, Thirumarimurugan, & Sivakumar, 2016). Manjari *et al*. used an aqueous extract of *A. elaeagnoidea* flowers and $Cu(NO_3)_2.3H_2O$ to make spherically shaped CuO NPs with a crystalline character. In the presence of sodium borohydride ($NaBH_4$), the resulting nanoparticles showed notable catalytic activity for the reduction of Congo red (CR), methylene blue (MB), and 4-nitrophenol (4-NP) at room temperature. The average particle size of CuO NPs produced in the 20-45 nm range was examined. Furthermore, even after two months of reaction, CuO NPs remained stable in aqueous solution, which could be attributed to the presence of different phytochemicals in the flower extracts around the CuO NPs. The phytogenic produced catalyst was easily recovered and reused for six consecutive cycles with a conversion efficiency of more than 90 % (Manjari et al., 2017).

2.3.2.2. Removal of Organic Dyes

Organic dyes are one of the most serious contaminants in polluted water (Das et al., 2018). Colored organic dyes have an impact on aquatic bodies because they block sunlight, lowering dissolved oxygen levels (Singh et al., 2019). Aminuzzaman *et al*. have reported that spherically shaped CuO NPs by using green waste of banana peels extract as reducing and stabilizing agents. The as synthesized NPs have high phase purity with average particles size of 60 nm. The results showed that well crystalline CuO NPs in nature, which have monoclinic phase. The biosynthesized CuO NPs revealed excellent photocatalytic degradation of Congo red, which is almost 90 % within 60 minutes, under direct sunlight (Aminuzzaman, Kei, & Liang, 2017). Muthuvel *et al*. have reported that the *Solanum nigrum* leaf extract intermediated synthesized CuO-NPs with better stability degraded the MB colorant at 97 % on irradiation with direct sun in around 50 minutes when compared to chemically synthesized CuO NPs (Muthuvel et al., 2020). Many papers have described the synthesis of copper oxide nanoparticles from various plant parts as a reducing and capping agents are illustrated in Table 1.

Table 1: Plant mediated CuO NPs for different applications

Biological entity	Pollutants	Efficiency (%)	Light source	Time (min)	Reference
Banana peel	Congo red	90	Sunlight	60	(Aminuzzaman

					et al., 2017)
Madhuca longifolia flower and seed	Methylene blue	77 and 46	Visible-light	150	(Das et al., 2018)
Lantana camara leaf	Methylene blue	94.07	sunlight	90	(Arunkumar, Jeyakumar, & Jothibas, 2019)
Solanum nigrum leaf	Methylene blue	97	Sunlight	50	(Muthuvel et al., 2020)
Citrofortunella microcarpa leaves	Rhodamin B	98	UV-light	100	(M. Rafique et al., 2020)
Moringa oleifera leaf	Pararosaniline	96.4	Sunlight	40	(Surendhiran et al., 2021)
Tecoma castanifolia leaf	4-Nitrophenol	100	Dark	14	(Sharmila et al., 2016)
Murayya koeniggi leaf	4-Nitrophenol	95.8	Dark	9	(Nordin & Shamsuddin, 2019)
Cordia africana Lam. leaf	4-Nitrophenol	100	Dark	12	(Bekru, Zelekew, Andoshe, Sabir, & Eswaramoorthy, 2021)
Cystoseira trinodis	Methylene blue	89 87	UV/ sunlight	-	(Gu et al., 2018)
Solanum lycopersicum leaf	Crystal violet	>97	Visible-light	300	(Vaidehi et al., 2018)
Psidium guajava leaf	Congo red Methylene blue	81 89	Sunlight	150	(Sathiyavimal et al., 2021)

In consideration of the above reports, no attempt was made to formulate the CuO NPs by onion peel extract. However, few researches show that the biogenic synthesized nanoparticles by using onion peel extract. Onion (*Allium cepa L.*) is the second most commonly consumed horticultural crop overall the world (Krishnasamy Sekar, Sridhar, Perumalsamy, Manikandan, & Ramasamy, 2020). It consists of several phenolic compounds, including quercetin, gallic acid, ferulic acid, protocatechuic acid, and kaempferol. The major flavonoid in the onion peel is quercetin which is mostly present in onion peel i.e., 20 times higher than the edible portion of onion. They have many health benefits includes cardiovascular and anticancer agents, with hypocholesterolemia, antioxidant, antiasthmatic, and antithrombotic activity (Ifesan, 2017) because of its flavonoid's contents (Lee et al., 2014). Onion bulb scales have higher concentration of oxygen-rich functionalities than in the leaves (Musyoka, Mutuma, & Manyala, 2020). However, onion peels usually discarded are environmental concern because they are unsuitable for organic fertilizer or fodder as result of their aroma and rapid development of phytopathogens characteristic (Kim, Kim, & Park, 2013). More than 500,000 metric tons of onion skin waste is discarded every year within the European Union (Musyoka et al., 2020). If not thrown away in the right way, it may contribute endangers to the environment (Ifesan, 2017). The abundant onion peel wastes generated across the world in organic synthesis, and thus help in reducing the environmental pressure (Chia, Lim, Yong, Poh, & Kan, 2018). In addition, Onion peel extract can be used as a reducing and capping agent for nanoparticles synthesis (Krishnasamy Sekar et al., 2020).

For instance, gold nanoparticles were developed using the dried outer peel of onion as a reducing and stabilizing agent. This was confirmed by the prepared powder put for one month but particles were not aggregated which suggested that Onion peel (OP) Au NPs were stable and capped well. The formulated OP-Au NPs had spherical and triangular shapes with an average size of 45.42 nm. OP-Au NPs displayed a strong synergistic antibacterial and anticandidal effects against various pathogenic microorganisms, as well as a strong antioxidant and proteasome inhibitory potential (Patra, Kwon, & Baek, 2016). Ag NPs by onion peel extract have also been the potential antipathogenic, antioxidant, and anti-proliferative activities. And also, onion peel extracts act as a reducing and capping agent. The as-synthesized NPs were a spherical in shape, cubic structure with an average particle size of 33-50 nm. The reduction of silver ions into silver NPs rapidly occurred within 30 min compared

to earlier reports (Krishnasamy Sekar et al., 2020). Spherically shaped ZnO NPs were synthesized by reduction of $Zn(CH_3COO)_2.2H_2O$ using onion peel extract as a reducing and capping agent (Canbaz, Açikel, & Açikel). Spherical-cubic nickel oxide nanoparticles were also synthesized by reducing nickel nitrate using Allium cepa peels and were applied to remedy the Congo red direct dye following the optimization of reaction conditions. The targeted dye was decolorized up to 90 % at dye concentration 0.02 %, catalyst dose 0.003 gL^{-1}, pH 6, and temperature 50 °C (M. A. Rafique et al., 2021).

Due to their inexpensive cost, natural abundance, high stability, and good electrical characteristics, copper oxide nanoparticles (CuO NPs) have recently gained importance among MNPs. Despite the benefits of CuO NPs, the small size and high surface energy of nanoparticles usually result in agglomeration, which is unavoidable. In order to avoid this problem, CuO NPs are frequently immobilized on solid supports, which are less expensive, such as cellulose, Graphene oxide, clinoptilolite, and others, which have successfully avoided aggregation and thereby increased the catalytic capabilities of CuO nanoparticles (Filiz, 2020).

2.4. CuO NPs with Different Support

2.4.1. Removal of Phenols and its Derivatives by Supported CuO NPs

Because catalytic activity is proportional to catalyst surface area, this outcome may result in a decrease in catalytic efficiency. As a result, they're usually loaded on a variety of supporting matrices or shaped into a specific structure, such as flower-like microsphere urchins or hollow nanospheres. Thus, new supporting materials for CuO NPs are of major scientific importance in order to fully exploit the exceptional catalytic functions of CuO NPs. (Z. Zhou et al., 2013). Copper is an excellent electrical conductor, therefore electrons can easily be transferred from one absorbed species to another on its surface. Copper's exceptional property makes it an excellent catalyst for the reduction of nitro compounds (Deka, Deka, & Bharali, 2014).

The catalytic performance of CuO NPs supported on a variety of metal oxides (ZrO_2, SiO_2, Al_2O_3, CaO, MgO, and ZnO) were evaluated in the reduction of 4-NP to 4-AP in an aqueous environment with excess Sodium borohydride. The influence of support material on the catalytic performance of CuO nanoparticles for the reduction of 4-NP was

also investigated, with the performance order of support being ZrO_2 > Al_2O_3 > SiO_2 > CaO > MgO > ZnO. The CuO/ZrO_2 catalyst demonstrated outstanding catalytic activity, with a pseudo-first-order rate constant of 15.97×10^{-3} s^{-1}. ZrO_2's dual sites were suggested to be capable of adsorbing and activating bonds and to function as dual sites for catalysis because of this (Filiz, 2020).

According to Zhou *et al*. the catalytic performance of the produced Cellulose nanocrystals (CNs) supported CuO NPs nanohybrids was assessed by reducing 4-NP with sodium borohydride ($NaBH_4$) to 4-AP. It reached around 100 % after 600 seconds, and the color bleaching rate was substantially faster than that of CuO NPs that were not supported (68.8 %). Because of their enormous surface area, the CNs-supported CuO NPs nanohybrids had much higher catalytic activity than the CuO NPs nanohybrids. However, the reaction rate of CNs-supported CuO NPs nanohybrids is slightly slower than that of CNs-supported Cu NPs nanohybrids. The reduction of GO to Graphene sheets by $NaBH_4$ results in GO-supported CuO NPs nanohybrids with strong catalytic activity, however the catalytic reaction rate remains constant until the completion of the reaction. Because of their much larger size and poor dispersion in solution, SiO_2-supported CuO NPs and Al_2O_3-supported CuO NPs displayed poor catalytic properties were used as comparisons in the study. Nevertheless, microcrystalline cellulose supported CuO NPs nanohybrids did not display significant catalytic activity due to the large size of microcrystalline cellulose, (MCC). Due to remarkable properties such as maintained physical and chemical structure, high catalytic activity when exposed to air for a week, easy preparation procedure, and low cost when compared to CNs-supported Cu NPs, it can be concluded that as-prepared CNs-supported CuO NPs are a feasible and efficient catalyst (Z. Zhou et al., 2013).

In addition, they discovered that hydrothermal method successfully created CuO nanoparticles homogeneously distributed across crumpled, paper-like surface of rGO, with excellent and steady catalytic reduction of 4-NP by changing the GO/Cu ratio. $CuO_{0.05}$-rGO had the highest catalytic activity in only 20 seconds, whereas $CuO_{0.01}$-rGO had the lowest catalytic activity and couldn't achieve the full reduction of 4-NP even after 18 minutes, whereas $CuO_{0.1}$-rGO only took 3 minutes at room temperature, as evidenced by the time-dependent UV-Vis absorption spectra. Thus, the CuO-rGO catalyst's catalytic activity is

dependent on both CuO and rGO. The catalytic activity increases as the amount of CuO increases, but at a certain amount, the activity drops. This could be because the available active surface of rGO for adsorption of 4-NP has decreased. For this reaction, the rate constant was estimated as 13.951 min^{-1}. Due to the loss of catalyst during the separation process, the rate constant (k) value of $CuO_{0.05}$-rGO nanocomposites has only slightly decreased after five cycles (Sarkar & Dolui, 2015).

According to Sharifi *et al*. *Rheum palmatum L*. root extract was utilized as a reducing and stabilizing agent, and copper oxide nanoparticles were disseminated on the surface of clinoptilolite. Natural clinoptilolite powder was ground into zeolite nanoparticles in a planetary ball mill. CuO NPs were made by heating Cu NPs in a furnace at 350 °C for 2 hours. The FTIR analysis of CuO NPs on clinoptilolite clearly shows that the functional groups do not change after CuO NP immobilization on clinoptilolite, confirming that organic compounds are absorbed on the surface of CuO NPs via electron interaction and act as both reducing and capping agents in the stabilization of prepared Cu NPs on clinoptilolite surface. CuO NPs/clinoptilolite showed good activity as a heterogeneous catalyst in the reduction of 4-NP, MB, and RhB in 150, immediately, and 60 seconds, respectively, at ambient temperature. Furthermore, this effective catalyst can be recycled up to five times, resulting in a 100 % reduction in pollutants (Bordbar et al., 2017).

2.4.2. Removal of Organic Dyes by Supported CuO NPs

The key issues in CuO-based photocatalysis includes suspension aggregation (Khan et al., 2020), absorption of visible light is rather low (Sapkota et al., 2020), and high e^-/h^+ recombination rate (Ganesan et al., 2020). To overcome these limitations, the catalyst immobilized onto suitable supports.

For instance, Sapkota *et al*. were synthesized a series of CuO-SWCNT nanocomposites (abbreviated as CuO-SWCNT-0.5, CuO-SWCNT-2, and CuO-SWCNT-5, where 0.5, 2, and 5 reflect the calcination duration in hours) using a cost-effective, simple recrystallization followed by calcination method. SWCNTs were surrounded by CuO nanocrystals via direct chemical bonding in the nanocomposites. All of the samples had excellent photocatalytic performance, but the CuO-SWCNT-5 photocatalyst had the best performance, decomposing

97.33 % of the MB in 2 hours. The development of heterojunctions between CuO and SWCNT improves separation and accelerates photoinduced electron-hole pair transfer. It also improves visible-light absorption, resulting in outstanding photocatalytic efficiency. The photocatalyst's recyclability was also studied; the catalyst could be reused three times without significant loss of catalytic efficiency or morphology (Sapkota et al., 2020).

Ganesan *et al*. were reported the fabrication of GO-CuO nanocomposites using *Acalypha Indica* leaf extract to make copper oxide nanoparticles (CuO-NPs), which were then dispersed around the Graphene oxide (GO) at random. Photocatalytic tests demonstrated that produced nanocomposites can destroy methylene blue dye with an efficiency of 83.20 % in 60 minutes, due to the inclusion of GO sheets, which accelerates the electron transport processes lot faster, hence increasing the rate of reactions dramatically, and has a narrow bandgap and a large surface area, which inhibits electron-hole recombination. Based on the aforementioned results as shown in Fig. 2, the proposed photocatalytic degradation mechanism for MB dye solution over CuO-GO nanocomposites was explained as follows. When UV–Visible light was used to irradiate CuO-GO nanocomposites, electrons were stimulated from the valence band (VB) to CuO's conduction band (CB), leaving holes in the valence band. These photoexcited electrons may travel from the CB to the GO surface during the photocatalytic activity, suppressing electron-hole recombination levels. In addition, photo-generated electrons and holes may react with water and oxygen molecules absorbed from the surface, forming reactive species that destroy dye molecules in solution (Ganesan et al., 2020). The significant contributions of copper oxide nanoparticles supported on suitable supports are summarized in Table 2.

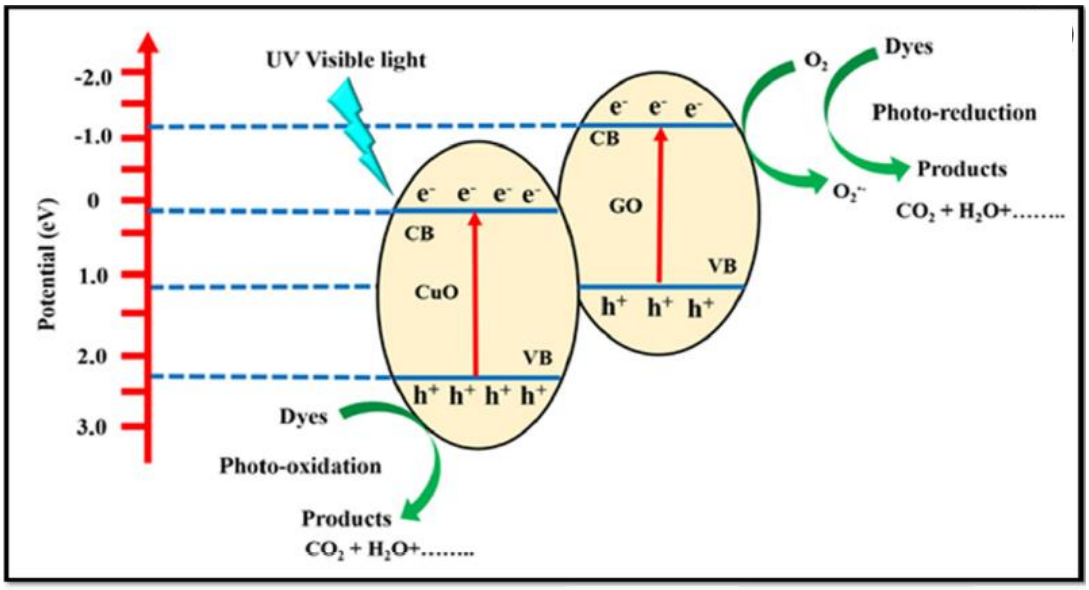

Fig. 2. Possible mechanism for dye degradation of MB with nanocomposites (Ganesan et al., 2020).

Table 2: The performance of the supported CuO NPs

Catalyst	Substrate	Light source	Rate constant or Efficiency	Time (min)	Reference
$CuO_{0.05}$-rGO	4-NP	Dark	13.951 min^{-1}	0.3	(Sarkar & Dolui, 2015)
CuO/Clinoptilolite	MB	Dark	-	Immediately	(Bordbar et al., 2017)
	RhB		-	1	
	4-NP		-	2.5	
CuO NPs@CNs	4-NP	Dark	0.414 min^{-1}	-	(Z. Zhou et al., 2013)
Cu NPs@CNs			0.468 min^{-1}	10	
CuO NPs@Al_2O_3			0.09 min^{-1}	8	
CuO NPs@SiO_2			0.228 min^{-1}	-	
CuO NPs@GO			0.204 min^{-1}	-	
CuO NPs@MCC			0.078 min^{-1}	-	

CuO/Al_2O_3	4-NP	Dark	0.684 min^{-1}	4	(Filiz, 2020)
CuO/ZrO_2			0.9294 min^{-1}	5	
CuO/SiO_2			0.3936 min^{-1}	10	
CuO/CaO			0.2988 min^{-1}	13	
CuO/MgO			0.2688 min^{-1}	15	
CuO/ZnO			0.231 min^{-1}	20	
CuO/rGO	MB	Visible	93 %	30	(Choi et al., 2017)
CuO-SWCNT-5	MB	Visible	97.33 %	120	(Sapkota et al., 2020)
CuO-GO	MB	Visible	83.20 %	60	(Ganesan et al., 2020)
CuO/rGO	MB	Visible	100 %	30	(Choi et al., 2017)
CuO/NC NPs	MO	UV/ visible	97.18/ 95.96 %	4	(Khan et al., 2020)

2.5. Layered Double Hydroxides (LDHs)

LDHs or hydrotalcite-like compounds are ionic lamellar materials made up of positively charged brucite-type sheets that are two-dimensional (Mahmoud, Moaty, Mohamed, & Farghali, 2017; Q. Wang & O'Hare, 2012). Anionic clays have a general formula of $[M^{2+}_{1-x} M^{3+}_x(OH)_2]^{x+}A^{n-}_{x/n}.mH_2O$. M^{2+} is made up of divalent cations that are replaced by M^{3+} trivalent cations, resulting in positive charges. Anions, represented by the letter A^{n-}, and water molecules make up the interlamellar gallery. Counter anions such as OH, CO_3^{2-}, Cl, and NO_3^- compensate the positive charges, (Jawad, Lu, Chen, & Yin, 2014; Palapa et al., 2020), oxyanions, halides, silicates, polyoxometalates, as well as complex and organic anions (Malak-Polaczyk, Vix-Guterl, & Frackowiak, 2010; Valdez, Grotjahn, Smith, Quintana, & Olivas, 2015), and polyacid anions (Xue et al., 2019) may be also used. The equations $M^{3+}/(M^{2+} + M^{3+})$ are used to calculate x (Zhao et al., 2018), which ranging from 0.2 to 0.33 for pure LDH formation (Shan et al., 2014). Metal ions are octahedral coordinated by six oxygen atoms from six OH groups (F. Li & Duan, 2006). The parent material for those compounds is

the mineral hydrotalcite, which has the formula $Mg_6A_{l2}(OH)_{16}CO_3.4H_2O$ (Malak-Polaczyk et al., 2010). Because the layers of LDHs are 0.48 nm thick, their structure is diverse (Fu, Zheng, Zhou, Ni, & Xia, 2019). LDHs can generate a variety of host-guest complexes due to their lamellar structure and anion exchange capability. The basal spacing of the LDHs increases when organic anions are incorporated into LDH interlayers, which is dependent on the nature, size, and geometrical structure of the intercalated species (Morimoto, Tamura, Iyi, Ye, & Yamada, 2011).

Another important property of LDHs is the "memory effect" refers to the structural restoration of the layered structure when the mixed metal oxides, formed after calcination at temperatures ranging from 300 to 600 °C, are exposed to aqueous solutions containing anions. MMO has a high adsorption capability. As a result, they can be used as adsorption materials, catalyst precursors, and catalytic supports with ease (Carja, Dartu, Okada, & Fortunato, 2013; Zhi et al., 2010).

Many scientific investigations have been conducted on these materials due to their capacity to retain diverse constituents while keeping the layered structural properties. These studies have revealed LDHs' multifunctionality and promise for use in a variety of fields; including medicine (Shahabadi, Razlansari, Zhaleh, & Mansouri, 2019), photo electrochemical water oxidation (Tang, Wang, Yang, Yan, & Xiang, 2016), agriculture (Tang et al., 2016), catalysis (Sangkhum, Yanamphorn, Wangriya, & Ngamcharussrivichai, 2019), and effluent treatment (Dumitru et al., 2019). Because of its great flexibility, high adsorption capacity, variable layer spacing and metal ion composition, efficient anion exchange capacity, ease of fabrication, large specific surface area and excellent thermal and chemical stability (Jawad et al., 2014; Moustafa, Mahmoud, El-Salam, & Shehata, 2021). LDH has been widely employed as an adsorbent, ion exchanger, and catalyst (Jawad et al., 2014; Palapa et al., 2020).

Under ideal wavelength range light irradiation, the valence electrons of LDHs with specific structures are stimulated into the conductive band and create electron-hole pairs, allowing LDHs to be employed as photocatalysts for the destruction of organic contaminants. Because the LDHs structure contains many water molecules and hydroxyl ions, which are required to create •OH radicals during photocatalytic oxidation, LDHs could be an excellent carrier for other high-performance catalysts (Fu et al., 2019).

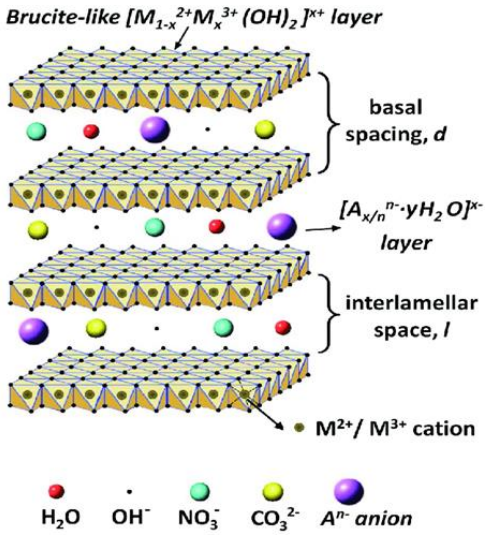

Fig. 3. General crystal structure of layered double hydroxide compounds (Scarpellini et al., 2014).

2.5.1. Synthesis Methods of LDHs

Numerous methods have been carried out on formation of layered double hydroxides such as urea hydrolysis, memory effect reconstruction, anionic exchange (Chakraborty, Sarkar, Haldar, Pal, & Chakraborty, 2015), mechanochemical (Z. Li, Chen, Ai, Wu, & Zhang, 2018), hydrothermal and Co-precipitation (Jiang et al., 2020). When compared to other procedures, each synthesizing method has its own unique advantages and limits. The co-precipitation process is the simplest and most widely used of all LDH synthesis techniques (G. George & Saravanakumar, 2017).

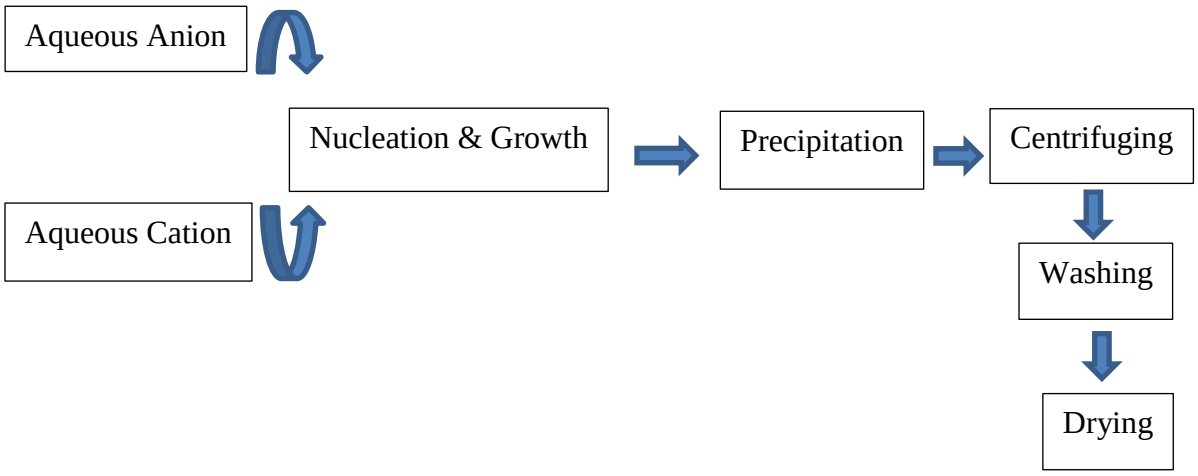

Fig. 4. Flowchart of Experimental Procedure (G. George & Saravanakumar, 2017).

2.5.2. Removal Efficiency of LDHs as Support

2.5.2.1. Degradation of Dyes

Seftel *et al*. produced TiO_2/MgAl-NO_3-LDH nanocomposites with a novel structure in which LDH crystallites are encased within an anatse TiO_2 matrix. Because the negatively charged surface of TiO_2 NPs at high pH attracts the cation dye MB during UV light irradiation, the nanocomposites showed higher photocatalytic activity in a basic environment as compared to standard Degussa P25 TiO_2. The advantages of the synthesized nanocomposites over pure TiO_2 include anatse crystals that are well dispersed on LDH without aggregation, a large surface area of anatse that is active sites for photocatalytic reactions, adequate exposure to organic pollutants due to unique structure, half of TiO_2 in the nanocomposites results in superior activity per mass, and the nanocomposites can be easily separated from suspension due to sediment in minutes (Seftel et al., 2010).

$Nb_2O_5.nH_2O$/LDH composites were also fabricated via hydrothermal synthesis of Nb_2O_5 microspheres followed by in situ growth of ZnAl-LDH shell. To make the Nb_2O_5@LDO catalyst, the obtained $Nb_2O_5.nH_2O$/LDH was calcined at 400 °C. The photocatalytic experiment results showed that the Nb_2O_5/LDO exhibits obvious photo activity, with Congo red degradation reaching a ratio of 85 % under visible-light irradiation due to outside LDO, but that Nb_2O_5 alone has no photocatalytic activity for Congo red because the surface charge of Nb_2O_5 is electronegative (MO-) under weak acid, neutral, or alkaline conditions (Huang et al., 2016).

Cu_2O/ZnAl-CLDH composites were effectively produced using ZnAl-CLDH as a precursor in a simple approach. The photocatalytic activity of the composites formed under visible light irradiation was high (90.18 %) at the optimum Cu/CLDH molar ratio of 1:1, calcination temperature of 500 °C, and initial MO concentration of 20 mg/L. According to the findings, Cu_2O nanoparticles with an average diameter of 500-1000 nm were evenly distributed on the surface or internal frame of ZnAl-CLDH to form the ZnO-Cu_2O heterostructure. Under the same conditions, the ZnO-Cu_2O heterostructure may effectively prevent photoelectrons and holes from recombination, resulting in greater photocatalytic activity for MO degradation than pure ZnAl-CLDH and pure Cu_2O. Because of its narrow

bandgap to absorb visible light, Cu_2O in the composites plays a crucial role in enhanced photocatalytic activity. In addition, because of its large surface area, ZnAl-CLDH has a high adsorption capability for MO molecules. The possible photodegradation mechanism of Cu_2O/ZnAl-CLDH composite has been proposed based on the above experimental results, as shown in Fig. 5. Under visible light irradiation, electrons in Cu_2O's valence band can be driven to the conduction band, leaving holes in the valence band. Due to the lower energy level of the conduction band in ZnO, photoelectrons may be able to transfer further. Cu_2O's valence band has holes in it, making it simpler for hydroxyl radicals ($^{\bullet}OH$) to form from OH groups absorbed on the surface. In addition, the absorbed molecular oxygen (O_2) scavenges the electrons that flow through ZnO, resulting in the formation of ($^{\bullet}O_2^-$) radicals. These radical groups of $^{\bullet}OH$ and $^{\bullet}O_2^-$ will induce the dissolution of MO. After three cycles, the composite showed good stability and reusability, with a MO degradation ratio of 80 % (X. Wu, Zhang, Jiao, & Wang, 2016).

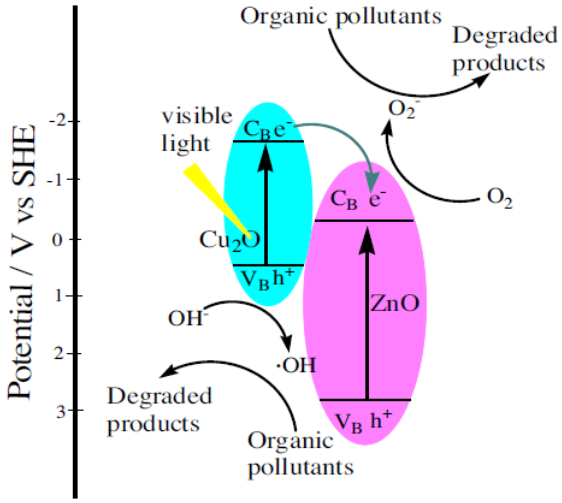

Fig. 5. Photodegradation mechanism of Cu_2O/ZnAl-CLDH photocatalyst under visible light irradiation (X. Wu et al., 2016)**.**

Zhang *et al.* have obtained CdS/MgAl LDH-precursor composites through mechanochemical operation in which CdS particles were successfully decorated among the matrix of Mg-Al LDH precursors rather than intercalated between the interlayers. When compared to pure CdS and pure LDH-precursor degrading the organic pollutant MB under visible light irradiation, the as-synthesized photocatalyst had significantly higher

photocatalytic activity. The composite photocatalyst was thought to be made up of CdS and MgAl-LDH, with CdS performing as a semiconductor photocatalyst and MgAl-LDH serving as a catalyst matrix but not a photocatalyst. Because MgAl LDH (precursor) was not a visible light photocatalyst, the MB dye degradation was entirely due to adsorption, even when exposed to visible light. Due to the surface coating of CdS on the LDH-precursor, the E_g values of 0.2CdS/LDH precursor, 0.5CdS/LDH-precursor, and CdS/LDH-precursor were all steady at 2.17 eV. The homogenous dispersibility of CdS on the LDH-precursor matrix, a crystallite size effect, and effective charge separation could all contribute to the improved photocatalytic effect (Z. Li et al., 2018). The photocatalytic processes of the CdS/MgAl-LDH are depicted in Fig.6.

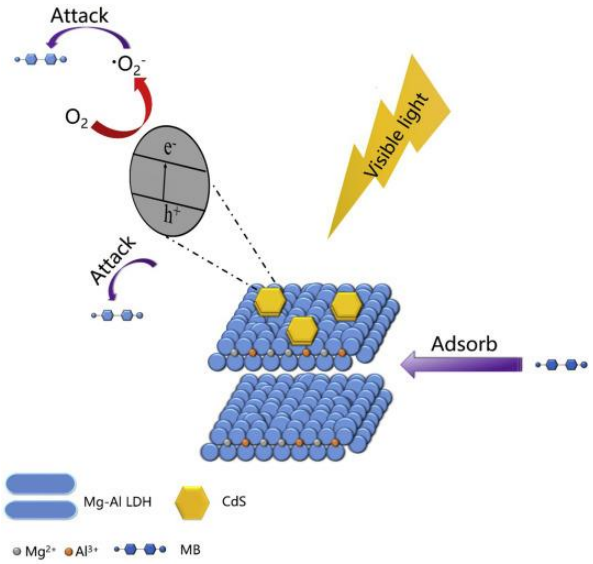

Fig. 6. Schematic diagram of the photocatalytic mechanism of the CdS/Mg-Al LDH (Z. Li et al., 2018).

Bhuvaneswari *et al*. reported glutathione-capped ZnS QDS with MgAl LDH hybrid as a photocatalyst against the degradation of MB dye under UV-Vis light irradiation, with the ZnS QDS uniformly anchored on the layered 2D LDH structure. When compared to bare ZnS QDS and bare LDHs, the hybrid showed improved photocatalytic degradation behavior. The ZnS QDs are principally responsible for this. It should be noted that the strong interaction with LDH assisted charge transport and improved the hybrid catalyst's photocatalytic performance. Furthermore, the LDH layer's surface OH groups react with valence band holes to produce

hydroxyl radicals (•OH) with a high oxidation potential, which are important factors in photo-oxidation reactions. ZnS QDs, LDH, and ZnS QDs-LDH hybrid had band gap values of 4.2, 2.17, and 2.78 eV, respectively (Bhuvaneswari, Palanisamy, Pazhanivel, Bharathi, & Nataraj, 2018).

2.5.2.2. Removal of Nitrophenol

A novel homogeneous and heterogeneous Au-Ag bimetallic nanocatalyst supported on MgAl LDH has been developed by Mehta *et al*. using a simple wet chemical procedure. Peak shifts were found in homogeneous catalysts as NPs content varied, but not in heterogeneous catalysts (almost the same peak position). For alloy (40-60 nm) and core-shell structure (15-30 nm) Au-Ag bimetallic nanoparticles supported on heterogeneous and homogeneous LDH composites, respectively, those catalysts are spherical but vary with average particle size. All homogeneous catalysts outperform heterogeneous catalysts when it comes to reaction rate. Au_3Ag_1 (both homogeneous and heterogeneous catalysts) had the highest activity of all the catalysts, which may be owing to its larger surface area, as determined by BET analysis. With 93 % efficiency, the catalysts may be utilized at least 5 times (Arora, Mehta, Mishra, & Basu, 2018).

Insin *et al*. used a simple method to make silver nanoparticles that were decorated on hydroxyapatite (Hap) and LDH. They used L-ascorbic acid as a reducing agent and TSC as a stabilizer and reducing agent. This immobilization might be achieved by hydrogen bonding between the surface hydroxyl groups of solid supports and the carboxylate groups of citrate ions, resulting in a catalytic activity that is stable, environmentally benign, reusable, and effective for 4-nitrophenol reduction. The number and particle size of Ag NPs had an impact on the catalytic performance of materials for 4-NP reduction. 4-NP was not diminished in the presence of bare Hap or LDH, as evidenced by the strength of the absorption peak at 400 nm remaining unaltered. Pure Ag NPs or Ag-based materials, on the other hand, were used to successfully reduce 4-NP to 4-AP using high-rate constants. The surface area of the Ag NPs-embedded substrates is double that of pure Ag NPs, despite the fact that the silver concentration in these materials was just 0.42 to 3.97 wt. %. As a result, the reactants were able to reach the catalysts and were easily reduced. Furthermore, only a limited number of active sites on the surface may be necessary for catalytic action. As the amount of silver in the

solution increased, the rate of reduction increased. Furthermore, the catalytic efficiency was unaffected by the solid support type. The rate constants of the same amount of Ag NPs on different supports were similar. This could be explained by the fact that silver was the reaction's sole active site. The enhanced catalytic efficacy of the composites compared to pure Ag NPs could be due to the Ag NPs distribution over the solid supports, which provided not only a large surface area of silver but also a high accessibility of the 4-NP to the active sites (Le Hoang et al., 2020).

Pd/MgAl LDHs were developed by ultrafine and highly dispersed palladium nanoparticles (Pd NPs) supported on exfoliated MgAl layered double hydroxide (Pd/LDH) catalysts, defect induced LDHs uniformly without agglomeration, by nitrogen glow discharge plasma reduction method without reducing agent and surfactant. The exfoliation and defects inducing of LDHs, and the reduction of palladium occurred simultaneously. The average Pd NP particle diameters of Pd/LDHs$_{30}$, Pd/LDHs$_{60}$, and Pd/LDHs$_{90}$ are 1.83 nm, 2.01 nm, and 1.94 nm, respectively. The Pd loading amount has no effect on size and morphology of Pd NPs and also on LDHs, but affect the dispersion of NPs. Prolonging N_2 plasma treating time, there are little effects on particle size of Pd NPs, but a significant change occurs to the morphology of LDHs and also introduce nitrogen atom in LDHs by destruct CO_3^{2-}. In addition, the interlayer spacing and crystallinity of LDHs decreased with duration of plasma treatment, due to the destruction of the interlayer anions and hydrogen bond of LDHs and crystal lattice defect introduced and exfoliated partially into ultra-thin nanosheet structure, respectively. The catalytic activity was improved by introduction of exfoliation and defects. The Pd/LDH catalyst with 1 wt. % Pd loading under nitrogen plasma treatment for 60 min showed the best catalytic performance in 4-nitrophenol reduction. The turnover frequency (TOF) of as-prepared catalyst is 20-fold higher than that of commercial Pd/C catalyst (Liu & Bai, 2021).

Table 3: LDHs-supported nanoparticles applications

Catalyst	Dyes	Light source	Removal rate/rate constant	Reaction time (min)	Reference
TiO_2/MgAl LDH	MB	UV-	-	-	(Seftel et al.,

		light			2010)
Cu_2O/Mg_7Al_5-LDH	Orange II	Visible-light	90 %	300	(Ma et al., 2015)
Cu_2O/ZnAl-CLDH	MO	Visible-light	90.18 %	420	(X. Wu et al., 2016)
Nb_2O_5@LDO	Congo Red	Visible-light	85 %	390	(Huang et al., 2016)
Cu_2O/MgAl-CLDH	MB	Visible-light	86.2 %	360	(Y. Zhou, Hu, Yu, & Jiao, 2015)
Cu_2O/MgAl-LDH	Orange II	Visible-light	90 %	300	(Ma et al., 2015)
Au/ZnCr-LDH	O-xylene	Visible-light	83.6 %	210	(Fu et al., 2019)
Au-Ag@MgAl-LDH NPs	4-NP	Dark	0.0375 min^{-1}(homo) 0.0285 min^{-1}(hetero)	30	(Arora et al., 2018)
TiO_2/MgZnAl-LDH	RhB MB 4-NP	Visible-light	93.73 % 85.88 % 89.33 %	540 480 240	(Zhao et al., 2018)
0.5CdS/MgAl-LDH-precursor	MB	Visible-light	94.78 %	90	(Z. Li et al., 2018)
ZnS-QDs-LDH hybrid	MB	UV-Vis light	95 %	120	(Bhuvaneswari et al., 2018)
Ag/MgAl-LDH	4-NP	Dark	0.32±0.029 min^{-1}	10	(Le Hoang et al., 2020)
Pd_1/MgAl-$LDHs_{60}$	4-NP	Dark	0.26 min^{-1}/ 98.07 %	14	(Liu & Bai, 2021)

These NPs could be more effectively stabilized by the suitable supports which hold their high surface area and catalytic activity. Among these support materials, Layered Double hydroxides (LDHs) is one of the most widely used supports and has gardening importance due to its intercalation properties. The support of LDHs would further reduce the size of NPs and hence prevent the agglomeration of NPs (Arora et al., 2018).

CHAPTER-THREE

3. EXPERIMENTAL METHODOLOGY

3.1. Chemicals and Reagents

All of the chemical reagents were of analytic grade: Copper nitrate trihydrate ($Cu(NO_3).3H_2O$), 95 % was purchased from LOBA CHEMIE PVT.LTD (India), Magnesium chloride hexahydrate ($MgCl_2.6H_2O$), and Aluminum nitrate nonahydrate ($Al(NO_3)_3.9H_2O$), 98 % and Sodium Bicarbonate ($NaHCO_3$), 99.5 % were purchased from Alpha Chemika (India), HCl (37 %), Sodium hydroxide (NaOH) was purchased from CENTRAL DRUG HOUSE (P) LTD (New Delhi), and Ethanol (96 %). The Fresh onion peels (Allium cepa L.) were collected from a cafeteria of ASTU. Distilled water (DW) was used throughout the experiment.

3.2. Methodology

3.2.1. Preparation of Plant Extract

A procedure similar to that described in (Krishnasamy Sekar et al., 2020) with modification was used to extract the plant. The onion peels were washed with distilled water several times before being dried at 85 °C. The dried onion peels were then cut in to small pieces. Five grams of onion peels were transferred to a flask and 350 mL distilled water were added, stirred and boiled at 70 °C for 30 minutes to get the aqueous extract. Then, the extract was cooled to room temperature, filtered through filter paper and kept at 4 °C for further use. Copper oxide was synthesized using the filtrate.

3.2.2. Phytofabrication Route of CuO NPs

CuO powder was prepared by Sol-Gel method by using Copper nitrate trihydrate ($Cu(NO_3).3H_2O$), Sodium hydroxide (NaOH) and *Allium cepa L*. peels extract based on the method of that described in the literature with modification (Sathiyavimal et al., 2021). As for the preparation of CuO NPs, 1.208 g $Cu(NO_3)_2.3H_2O$ (0.05 M) was dissolved in 100 mL of distilled water and then added to an aqueous extract of onion peel (100 mL) under vigorously stirred for 45 minutes at room temperature. Then aqueous NaOH (0.5 M) was added to attain a pH of 10. The entire reaction was carried out at 70 °C for 3 hours with constant stirring. CuO formation was confirmed by the appearance of dark green colored precipitates. The solutions

were aged for 24 hours before being centrifuged and dried overnight at 80 °C. Finally, powder sample was calcined in a furnace for 2 hours at 400 °C.

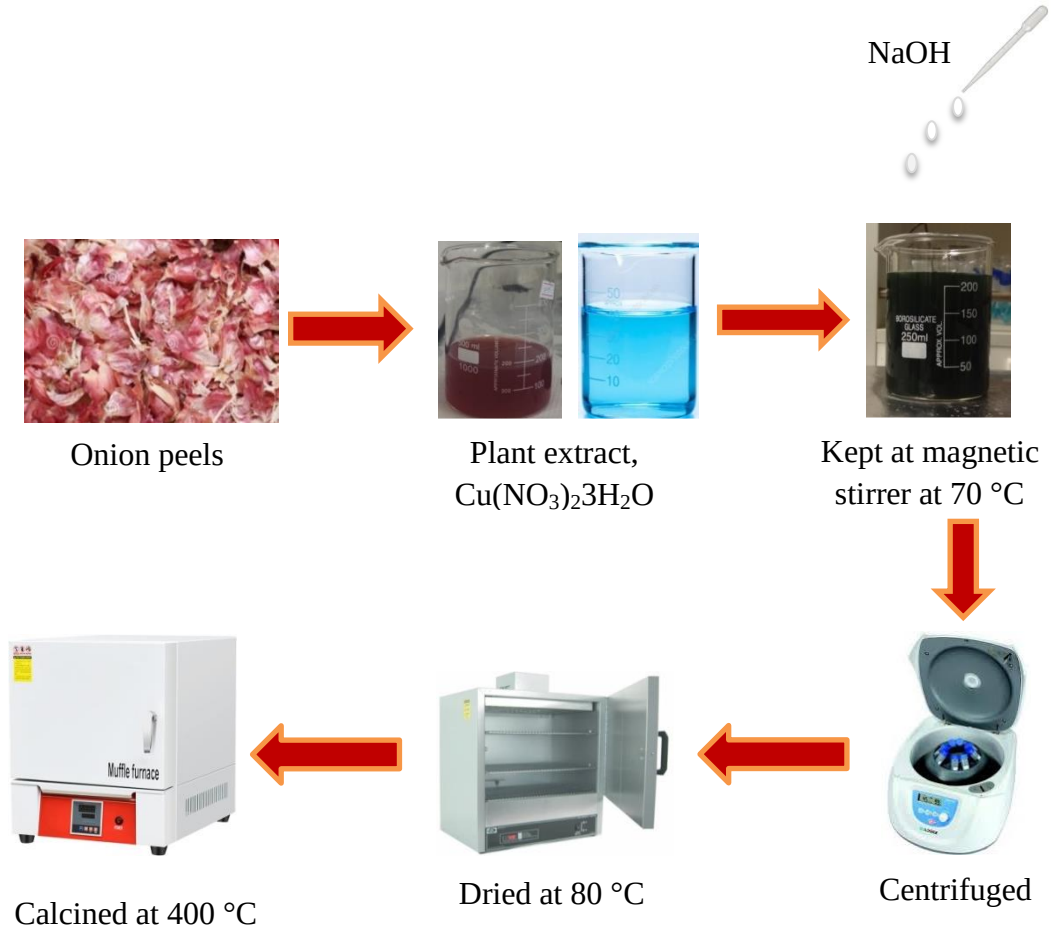

Fig. 7. Green synthesis of CuO nanoparticles by *Allium cepa L.* peel extracts.

3.2.3. Preparation of MgAl-LDHs

The MgAl-LDH was synthesized by a reported method with modifications (Nayak & Parida, 2016). MgAl-LDH was carried out using a co-precipitation method with an Mg^{2+}/Al^{3+} molar ratio of 3:1. Briefly, an aqueous solution containing 1 M solution of NaOH and 0.075 mole of $NaHCO_3$ was added dropwise to a vigorously stirred aqueous salt solution of $MgCl_2.6H_2O$ (0.015 mole) and $Al(NO_3)_3.9H_2O$ (0.005 mole) at 60 °C. The pH of the metal salt solutions was set to 9 and the reaction was performed under continuous stirring for 2 hours. The resulting precipitate was extensively rinsed with deionized water and ethanol until the pH

was neutral, after being aged at 60 °C for 12 hours. The solid residue was collected and dried at 80 °C for 12 hours.

3.2.4. Preparation of CuO/MgAl LDHs Nanocomposites

Co-precipitation was used to prepare the CuO NPs/MgAl-LDH (1:2) composite catalyst. To obtain a uniform suspension, the prepared CuO (0.3077 g) was ultrasonically dispersed in 100 mL distilled water in a 500 mL beaker for 1 hour, and then placed in a 60 °C water bath with stirring. Then the prepared CuO suspension was added dropwise into a salt solution containing 0.192 g $MgCl_2.6H_2O$ and 0.2424 g $Al(NO_3)_3.9H_2O$. To keep the pH around 9, 4 g NaOH and 6.30075 g $NaHCO_3$ were added. The precipitate was aged for 8 hours and then washed with distilled water until the solution became neutral. Finally, the composite was dried overnight at 80 °C (Shan et al., 2014). Different amounts of CuO and MgAl-LDH solutions with different CuO and MgAl-LDH weight ratios were prepared and designed as 1:1 and 2:1, respectively.

3.3. Photocatalytic Activity

The photocatalytic activities were measured by the degradation of methylene blue in a photocatalytic reaction chamber using 250 W halogen lamps. Before exposing to visible light, 25 mg of photocatalyst was mixed with 100 mL of methylene blue (MB) dye solution (10 mg/L), and stirred for 30 minutes to establish an adsorption-desorption equilibrium in a dark environment (It's worth noting that the change in dye concentrations was utilized to calculate the dye adsorption level in the dark). The combination suspension was then kept under regular stirring and visible light irradiation. To analyze dye degradation in the presence of photocatalyst, a 5 mL aliquot was collected from the mixed suspension following every 20 minutes of reaction time, centrifuged for 15 minutes at 5,000 rpm to get a clean supernatant solution containing the dye, and lastly scanned through the wavelength range of 200 to 800 nm using the Shimadzu-3600 plus UV-Vis spectrophotometer. MB had a maximum wavelength of 664 nm. The absorbance of dye was used to determine the concentration of leftover dye after the photocatalytic experiment. The following equation was used to calculate the photocatalytic degradation efficiency (%) of photocatalysts (Kannan et al., 2022):

$$D\ (\%) = [(C_0 - C)/C_0] \times 100\ \% \quad (3)$$

, Where C_0 is initial concentration of MB (mg/L) at t=0 and C is the remaining concentration of MB in aqueous solution at time (mg/L).

3.4. Characterization Techniques

A UV-visible spectrophotometer was used to measure spectra in a quartz cuvette from 200 to 800 nm (Shimadzu-3600). The bonding and functional groups of the samples were investigated using Fourier transforms infrared spectroscopy (FTIR-6600 type A) from 4000-400 cm^{-1}. X-ray photoelectron spectroscopy was used to determine the products' surface chemical composition (XPS, PHI-5700 ESCA system). The morphologies of the samples were examined by field-emission scanning electron microscopy (FESEM, JSM 6500F, JEOL) and transmission electron microscopy (TEM) (FEG TEM technai G2 F30). Crystallographic studies of samples were carried out with Cu Kα radiation source (λ=1.5406 Å) on X-ray powder diffraction (Shimadzu XRD-7000) from 2θ = 10° to 80°. Photoluminescence (PL) Spectroscopy of a JASCD FB-8500 can be used for determining the separation efficiency of photogenerated electron and hole pairs. The optical absorption was analyzed using UV-Vis diffuse reflectance spectroscopy (DRS) of Shimadzu UV-3600 to determine the band energy position, with a blank sample of $BaSO_4$ serving as a reference, wavelengths ranging from 300 to 800 nm.

CHAPTER-FOUR

4. RESULTS AND DISCUSSIONS

4.1. XRD Analysis

The XRD patterns of CuO NPs, MgAl-CO_3^{2-} LDH, and CuO/MgAl-LDH with different weight ratios of 2:1, 1:1 and 1:2 are shown in Fig. 8. In Fig. 8a, the characteristic reflections at 32.42°, 35.47°, 38.68°, 48.76°, 53.43°, 58.16°, 61.51°, 66.07°, 67.89°, 72.29°, and 75.00° correspond to the crystal planes (110), (-111), (111), (20-2), (020), (202), (11-3), (31-1), (113), (311), and (004), respectively. The strength of the (-111) and (111) peaks is significantly higher than that of the other peaks, indicating that the produced nanocrystals prefer to align in these orientations (A. George et al., 2022). The absence of peaks in the pattern corresponding to $Cu(OH)_2$ and Cu_2O, as well as the existence of all peaks corresponding to the monoclinic CuO phase (JCPDS Card number 00-048-1548, C2/c space group) is consistent with these values, indicates that pure crystalline CuO was formed (Bekru et al., 2021).

As shown in Fig. 8b, the well-organized and highly oriented two dimensional layer stacking of the produced LDH is suggested by the sharp and symmetric properties of the Bragg reflections corresponding to the (*00l*) planes with interlayer carbonate anions (Bhuvaneswari et al., 2018; Zheng et al., 2019). The MgAl-LDH reflections with peaks at 2θ=11.44° and 23.03°, matching to (003) and (006) crystal planes of $Mg_6Al_2(OH)_{18}.4.5H_2O$ (JCPDS No. 22-0700), were attributed to hydrotalcite type materials in a hexagonal lattice with R-3m rhombohedra symmetry (Z. Li et al., 2018), confirming the production of LDH crystals with good phase purity. The high intensity of these distinctive peaks indicated a high degree of crystallinity (Chang et al., 2013). The diffraction peaks at 11.44°, 23.03°, 34.75°, 39.06°, 46.41°, 60.54°, and 61.78° correspond to (003), (006), (009), (018), (015), (110), and (113), respectively.

When the prepared CuO NPs were uniformly loaded on the MgAl-LDH surface, the XRD patterns (Fig. 8c, d and e) of the composites mainly exhibited the features of copper oxide; some diffraction peak signals of MgAl-LDH were screened, which may be due to its small particles, high signals, and low crystallinity. However, MgAl-LDH as a carrier did not affect the structure of CuO NPs (Y. Wang et al., 2018). Impurity peaks were no longer found.

The XRD patterns clearly show characteristic diffraction peaks for both the LDH and monoclinic phases. The crystallite sizes of the samples were calculated using the Scherrer equation (Patel, Mishra, Verma, & Shikha, 2022):

$$D = \frac{K\lambda}{\beta Cos\theta}, \quad (4)$$

Where D is the size of the crystallite, λ is the wavelength of the X-ray source used (λ=0.15406 nm for Cu Kα radiation), β is the width (in radians) of the peak at half its height (FWHM), θ is the Bragg angle, and k is the shape constant of 0.9. The average crystallite size of CuO, MgAl LDH, and CuO/MgAl LDH (1:2, 1:1, 2:1 wt. %) was determined to be around 9.69 nm, 6.63 nm, 9.15 nm, 12.02 nm and 9.74 nm, respectively.

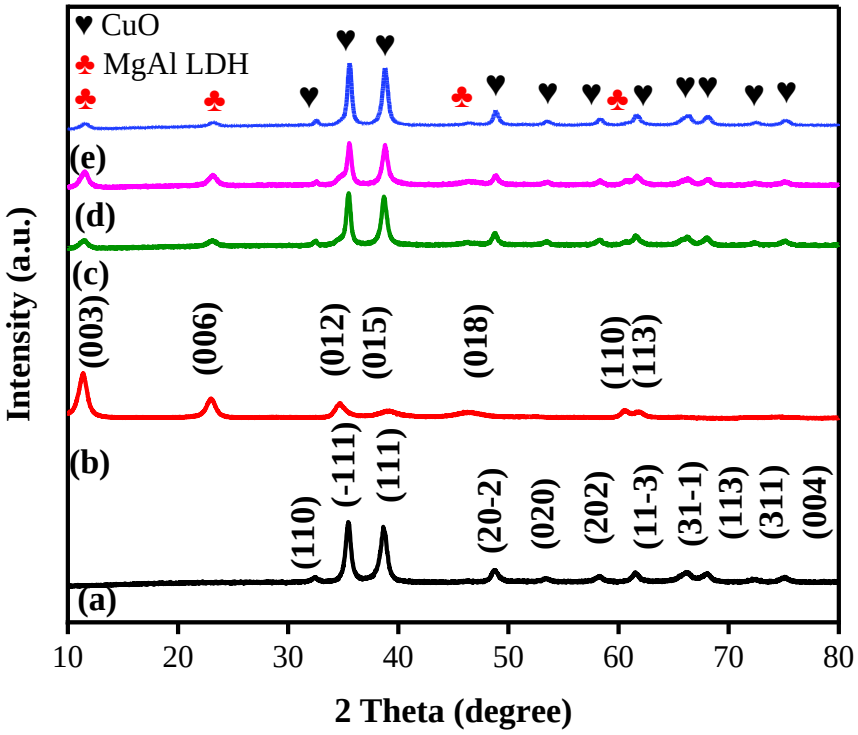

Fig. 8. XRD patterns of the (a) CuO NPs, (b) MgAl-LDH, (c) CuO/MgAl-LDH (1:1), (d) CuO/MgAl-LDH (1:2), and (e) CuO/MgAl-LDH (2:1).

4.2. FTIR Analysis

The functional groups of as-prepared CuO NPs, MgAl-LDH and CuO NPs/MgAl LDH (1:2) samples were investigated by FTIR spectroscopy in the range of 400-4000 cm^{-1}. As shown in the Fig. 9a and b, the O-H stretching vibrations, H-bonds of the alcohols, and phenol groups of the substances were represented by absorption band at 3427 cm^{-1} in the onion peels

extract, which was shifted to 3434 cm^{-1} in the case of the CuO NPs. The existence of carbonyl amide I vibrations and N-H bending of the main amine groups caused the band at 1626 cm^{-1} in the onion peels extract. Because of the proteins/peptides and amino acids present in the onion peels extract, which may have been implicated in the capping and reduction of Cu^{2+} to Cu NPs via the amine groups, this band was moved to 1635 cm^{-1} in the case of CuO NPs (Patra et al., 2016). The stretching vibration of methyl is represented by the weak band peak at 2922 cm^{-1} (Krishnasamy Sekar et al., 2020). An asymmetric stretching of C-O occurs in cyclic polyphenol compounds, resulting in the band at 1244 cm^{-1} (Lem et al., 2021). The reduction of Cu NPs was seen when distinct functional groups in CuO NPs were shifted from the Onion peel stretching (Patra & Baek, 2015). The bands emerging from the vibrational frequencies of the metal-oxygen (M-O) connection are usually seen below 1000 cm^{-1}. Hence, the peak positioned at 727 cm^{-1} belongs to characteristic vibrations of Cu-O bond, revealing CuO NPs formation (Bekru et al., 2021). In this study, the resulting CuO nanoparticles may have been formed by these groups acting as a reducing agent. Therefore, FTIR analysis investigated flavonoids, phenolic, methyl, amide groups, and proteins that are engaged in the reduction of metal precursor, preventing agglomeration, and acting as a capping agent.

In the Fig. 9c, the stretching modes of O-H groups associated to metal cation bonds in the hydroxide layer, as well as stretching vibrations of interlayer water molecules, can be attributed to the strong and broad absorption peak at 3440 cm^{-1} in pure MgAl-LDH (Nayak & Parida, 2016; Shan et al., 2014). CO_2 from air is usually allocated to the band at 2337 cm^{-1} (Zaghloul et al., 2019). The asymmetric vibration of CO_3^{2-} anions and the bending vibration of water molecules between layers in the interlayer region affected the peaks at 1345 cm^{-1} and 1622 cm^{-1}, respectively, while the presence of C-O and C=O bonds might cause the CO_3^{2-} peak to break (X. Li et al., 2019; Zheng et al., 2019). The vibrations of M-O/M-O-M (M=Mg, Al) characteristic of the double-lamellar structure are responsible for the remaining bands below 1000 cm^{-1} (Kerchich, Boudjemaa, Chebout, Bachari, & Mameri, 2021). The CuO/MgAl-LDH (1:2) spectrums comprised all feature bands of CuO NPs and MgAl-LDH, as shown in Fig. 9d. As a result, copper oxide could be spread on the LDH's surface. The FT-IR results confirmed that the desired composites had been made.

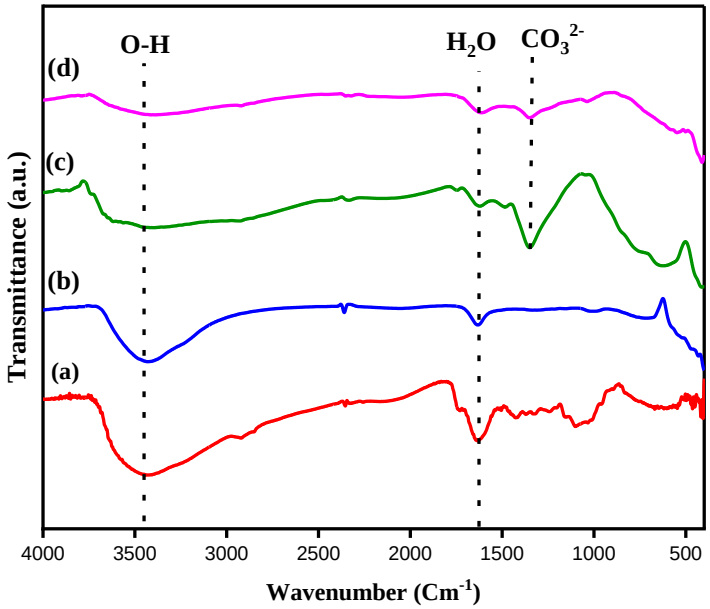

Fig. 9. FTIR spectra of (a) *Allium cepa.L* peels extract, (b) CuO NPs (c) MgAl-LDH and (d) CuO/MgAl-LDH (1:2).

4.3. XPS Analysis

X-ray photoelectron spectroscopy (XPS) was used to investigate the chemical states of the elements present in the CuO NPs/MgAl LDH (1:2) nanocomposites. The XPS survey scan (Fig. 10) revealed the presence of Cu, Mg, Al, and O elements, which is consistent with the EDS data (Fig. 11d). Two main peaks at 933.8 and 953.8 eV, which correspond to the Cu $2p_{3/2}$ and Cu $2p_{1/2}$, respectively, can be seen in the Cu 2p core level spectrum shown in Fig. 10a, indicating the presence of the Cu^{2+} chemical state in CuO particles. The distance between these Cu 2p main peaks is 20.0 eV, which is consistent with previous CuO spectrum reports. Furthermore, the broad satellite peaks at a higher binding energy than the main peaks provided additional confirmation of the CuO state. Cu $2p_{3/2}$ had accompanied by two satellite peaks on the higher binding energy side at around 943.8 eV and 941.5 eV, indicating the presence of CuO. The main peak of Cu $2p_{1/2}$ at 953.8 eV and its satellite peak at 962.5 eV were separated by about 9.0 eV, confirming the presence of CuO, as shown in this figure (Yuan et al., 2018). The satellite peak at around 943.8 eV clearly demonstrates an open $3d^9$ shell, thus supports the presence of Cu^{2+} in the sample, which is positioned at higher binding energies than the main peaks (Choi et al., 2017; Z. Zhou et al., 2013). The high resolution spectrum of Mg 2p is presented in Fig. 10b. In the Mg 2p spectra, single peak appear at 49.6 eV, corresponding to

Mg^{2+} in the brucite layers of MgAl-LDH (J. Chen et al., 2020). The Al 2p spectrum, deconvoluted into two peaks at 75.15 and 77.15 eV, can be assigned to Al 2p (α) and Al 2p (β) of $Al(OH)_3$ and Al_2O_3, respectively, emerging from the LDH structure, as shown in Fig. 10c (Bhuvaneswari et al., 2018). The binding energy of 529.4 eV belongs to lattice oxygen (O^{2-}) in the O 1s spectrum (Fig. 10d), while the peak at 531.6 eV reflects defects, chemisorbed oxygen, and coordinated lattice oxygen (Zhen et al., 2019).

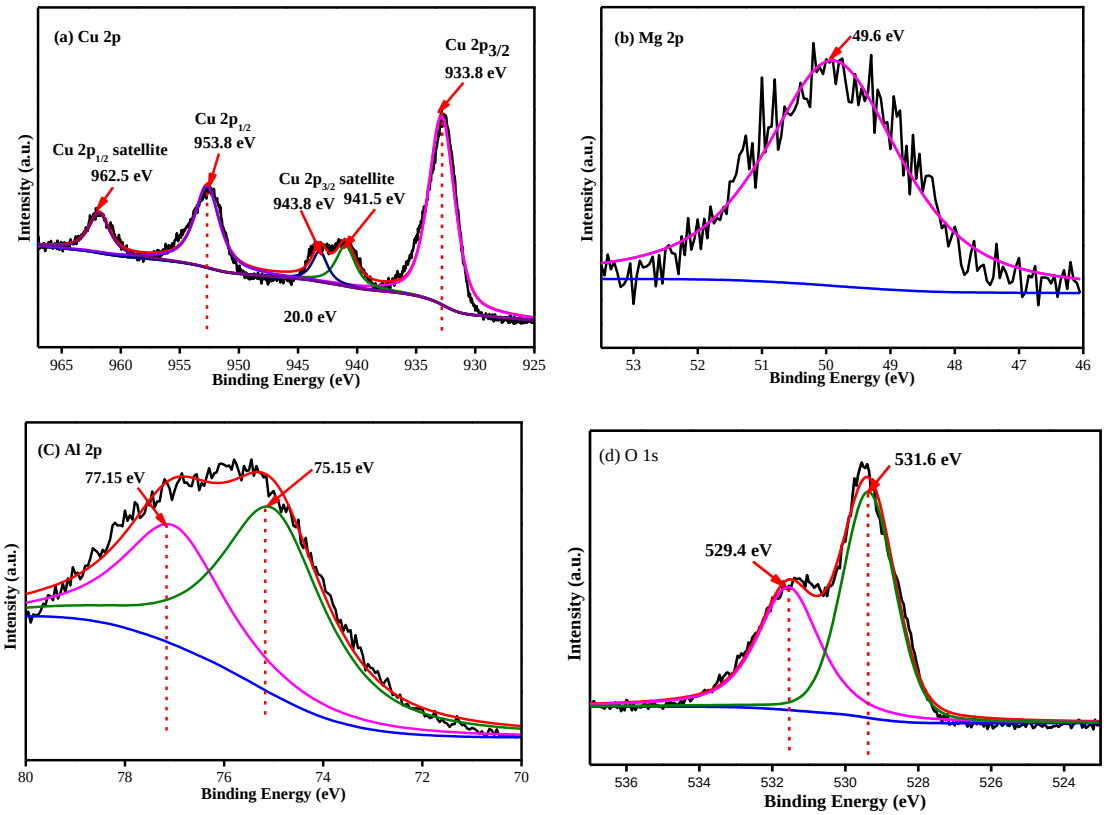

Fig. 10. High-resolution XPS spectra of Cu 2p (a), Mg 2p (b), Al 2p (c), and O 1s (d) of CuO/MgAl-LDH (1:2).

4.4. SEM/EDS Analysis

Typical FESEM/EDS images of the samples are shown in Fig. 11a-d. The microscopic morphology of pure CuO NPs had a definite spherical-like morphology as rough agglomerate is displayed in Fig. 11a. The biogenic production of CuO NPs produces very tiny spherical particles with different size. Small nuclear particles agglomerate and organize themselves into larger spheres (Veisi et al., 2021). The prepared MgAl-LDH with a typical flat, sheet-like structure is shown in Fig. 11b. The SEM micrographs of the CuO NPs/MgAl-LDH (1:2)

composites are shown in Fig. 11c. CuO NPs were uniformly and densely loaded on the surface of nanosheets, as can be seen. The energy dispersive spectroscopy (EDS) spectrum of CuO/MgAl-LDH (1:2) (in Fig. 11d) reveals the presence of Mg, Al, O, and Cu elements, as well as their wt. % composition is 18.76, 7.53, 47.53, and 26.18, respectively; these values indicated that the estimated atomic ratio of Mg to Al was ~3:1 with an experimental error, further confirmed the CuO/MgAl LDH composite's synthesis.

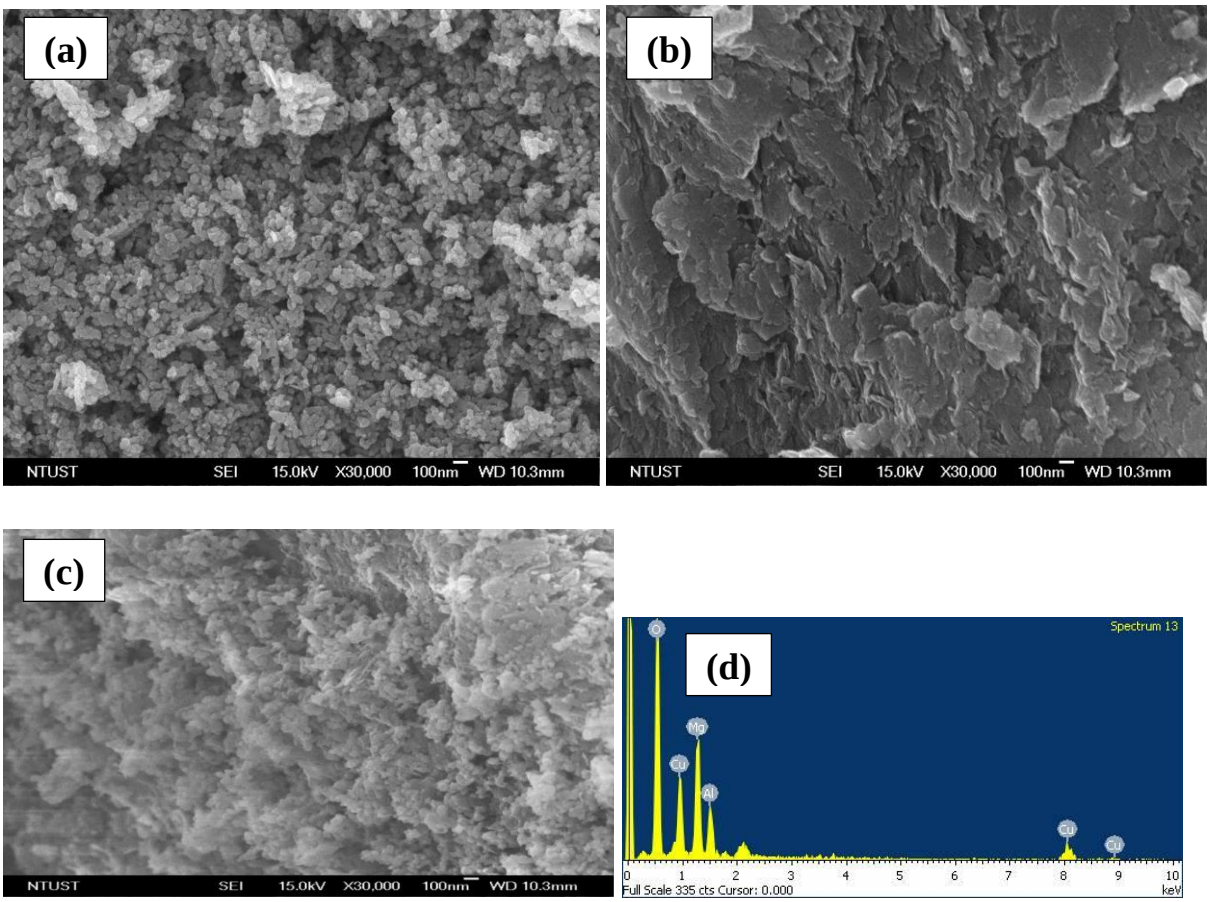

Fig. 11. SEM spectrum of (a) CuO nanoparticles, (b) MgAl-LDH, (c) CuO/MgAl-LDH (1:2) and (d) EDS spectra of CuO/MgAl-LDH (1:2).

4.5. TEM Analysis

More detailed information on the microstructure and shape of the CuO/MgAl-LDH (1:2) nanocomposites was obtained using transmission electron microscopy (TEM), as shown in Fig. 12. TEM image (Fig. 12a) confirms dark spots of CuO nanoparticles were distributed on the light gray matrix of LDH. The d-spacing of particles adhered to the surface of the LDH

support is 0.234 nm, according to the HRTEM image (Fig. 12b), which belongs to the CuO phase's (111) plane, revealing the composites texture of the nanosized CuO-layered double hydroxide clay matrix.

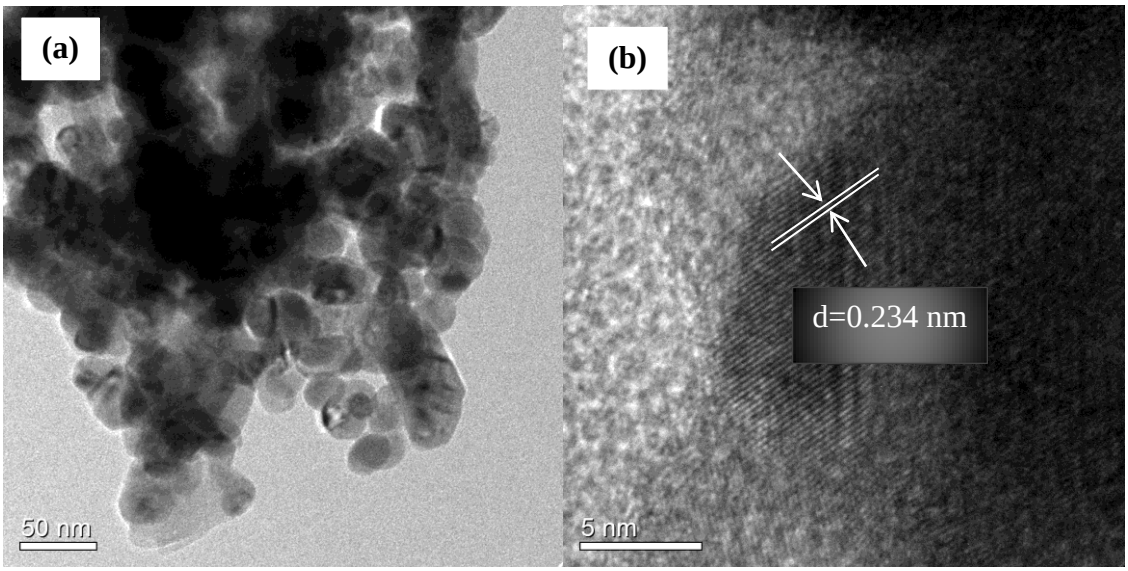

Fig. 12. TEM (a) and HRTEM (b) images of CuO/MgAl LDH (1:2) nanocomposites.

4.6. UV-Vis Diffuse Reflectance Spectra Analysis

The optical properties of the produced materials were characterized using UV-Vis DRS, and the results are recorded in Fig. 13a-d. The Kubelka-Munk method is used to calculate the corresponding bandgap of samples (J. Chen et al., 2020):

$$(\alpha h\vartheta)^n = K(h\vartheta - E_g) \quad (5)$$

where α is the absorption coefficient, $h\vartheta$ is the incident photon, *K* is the absorption constant, E_g is the optical bandgap energy, and n=2 for direct allowed transitions while it is ½ for indirect allowed transitions (Kerchich et al., 2021). The change of $(\alpha h\vartheta)^{1/2}$ vs. $h\vartheta$ for the samples reveals that the energy gap of the indirect band gap is obtained by extrapolating the linear part to the $h\vartheta$ axis. The calculated bandgap energy values of CuO NPs, CuO/MgAl-LDH (1:1), CuO/MgAl-LDH (1:2), and CuO/MgAl-LDH (2:1) are 1.66, 1.71, 1.82 and 2.35 eV. The result can be explained that the anionic clays LDH, which have abundant $^{-}$OH groups could promote electron transfer, so composites have efficient utilization in visible light compared to pure CuO. This is also attributed to the nanocomposites formation. With a larger

optical response range, the CuO NPs/MgAl-LDH (1:2) composite is expected to have better photocatalytic activity than its pure counterparts.

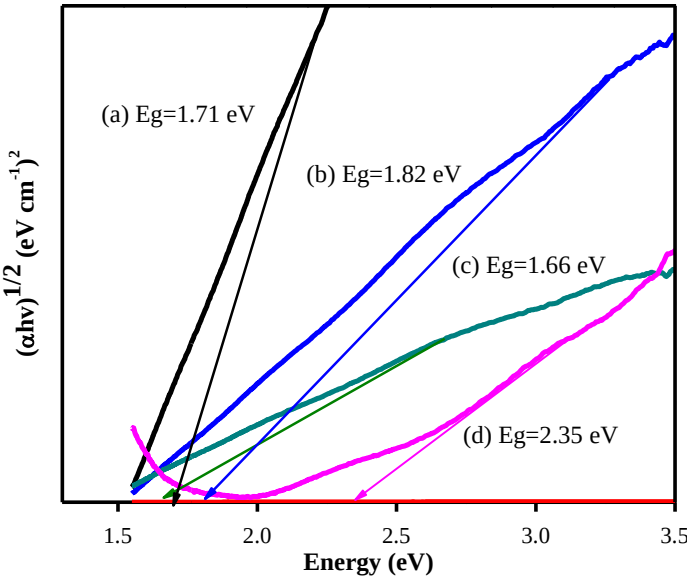

Fig. 13. The corresponding energy band gaps of (a) CuO/LDH (1:1), (b) CuO/LDH (1:2), (c) CuO NPs, and (d) CuO/LDH (2:1).

4.7. Photoluminescence Spectroscopy (PL) Analysis

The PL spectrogram analysis is crucial for determining how well-photogenerated electrons and holes pairs are separated in a photocatalyst. The recombination rate of photogenerated carriers has a significant impact on photocatalytic characteristics (X. Li et al., 2019). The steady-state PL emission spectra of pristine CuO and MgAl-LDH, and CuO/MgAl-LDH (1:2) composite stimulated at 300 nm. The PL emission peak of CuO/MgAl-LDH (1:2) is substantially reduced, indicating a much higher separation efficiency of photoinduced charge carriers than bare samples (J. Chen et al., 2020). The rate of recombination of excited electron-hole pairs determines the intensity of PL emission. Higher intensity indicates a faster rate of recombination of excited electrons, while lower intensity indicates a large amount of transferred or trapped electrons. As shown in Fig. 14, CuO/MgAl-LDH (1:2) composites have much lower emission intensity than both. This indicates that the recombination of photogenerated electron-hole pairs in the CuO/MgAl-LDH (1:2) composite was effectively inhibited (Ni et al., 2018). The composite's strongest photocatalytic activity was matched by its lowest electron-hole pair recombination rate by extending the lifetime of photogenerated charge carriers (X. Li et al., 2019).

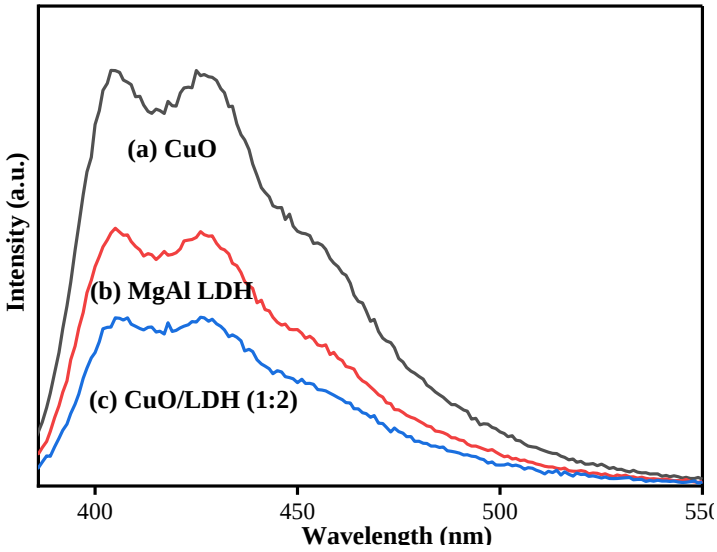

Fig. 14. Photoluminescence (PL) spectra of (a) CuO NPs, (b) MgAl-LDH and (c) CuO/LDH (1:2).

4.8. Photocatalytic Activity

The potential of synthesized samples for photocatalytic degradation of MB dye were examined under visible light irradiation. Typically, MB showed its original absorption peak at 664 nm. As shown in Fig. 15a-e, a time-dependent decrease in the dye's absorption band intensity was observed after the addition of photocatalyst. Under the same experimental conditions, all CuO/MgAl-LDH composites outperformed pure CuO NPs in terms of degradation efficiency.

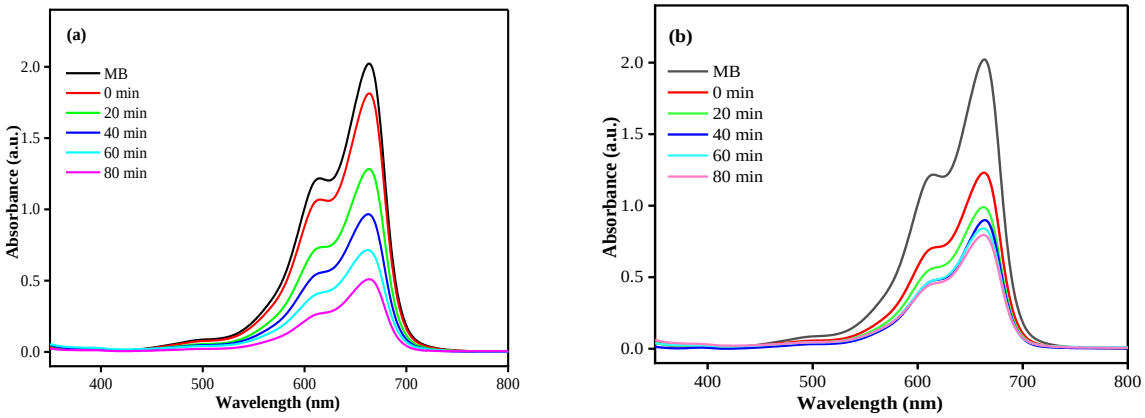

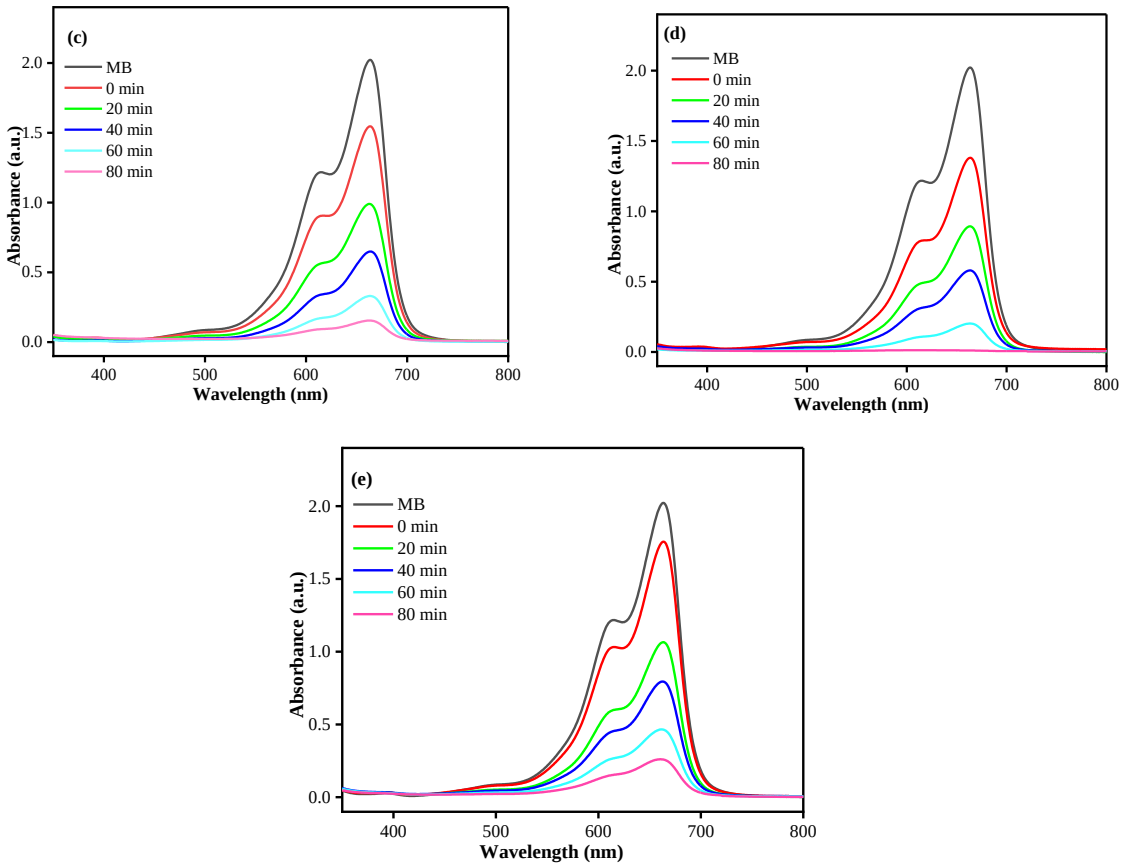

Fig. 15. UV-Vis absorption spectra for MB degradation catalyzed by (a) CuO NPs, (b) MgAl-LDH, (c) CuO/MgAl-LDH (1:1), (d) CuO/MgAl-LDH (1:2), and (e) CuO/MgAl-LDH (2:1).

The degradation of MB under visible light irradiation was used to test the photocatalytic behaviors of CuO NPs, MgAl-LDH, CuO NPs/MgAl-LDH (1:1), CuO NPs/MgAl-LDH (1:2) and CuO NPs/MgAl-LDH (2:1) samples, and the findings are shown in Fig. 16. In the absence of a photocatalyst, the degradation of MB is almost negligible throughout the blank experiment. The MB degradation study was activated by dispersion of 0.025 g of the catalyst in 10 ppm of MB (100 mL) under visible light irradiation for 80 minutes. The photodegradation efficiency of MB by CuO NPs/MgAl-LDH (1:2) is around 99.20 %, which is greater than that of MgAl-LDH, CuO NPs, CuO NPs/MgAl-LDH (2:1) and CuO NPs/MgAl-LDH (1:1) which are respectively 35.53 %, 71.87 %, 85.30 %, and 90.03 %.

Furthermore, MgAl-LDH demonstrated high adsorption of MB molecules in the dark when achieving the equilibrium adsorption state and a low visible light photocatalytic activity of MB molecules when exposed to visible light. It can be attributed to MgAl LDH's large

surface area and low visible light absorption. Zhou *et al*. discovered a similar occurrence, which they attributed to the large surface area of MgAl LDH (Y. Zhou et al., 2015). The CuO NPs sample, on the other hand, has reduced adsorption of MB molecules and higher photocatalytic activity. The findings suggest that CuO NPs is critical for photocatalytic activity and that adding CuO NPs into MgAl-LDH could boost photocatalytic activity. CuO/MgAl-LDH (1:2) nanocomposites have higher activity than CuO NPs due to uniform deposition of CuO NPs on the surface of MgAl-LDH, which increases CuO NPs surface area and has a synergistic effect in reducing the recombining rate of charge carriers, as well as quick dye adsorption on MgAl-LDH followed by rapid photodegradation, by supported CuO NPs.

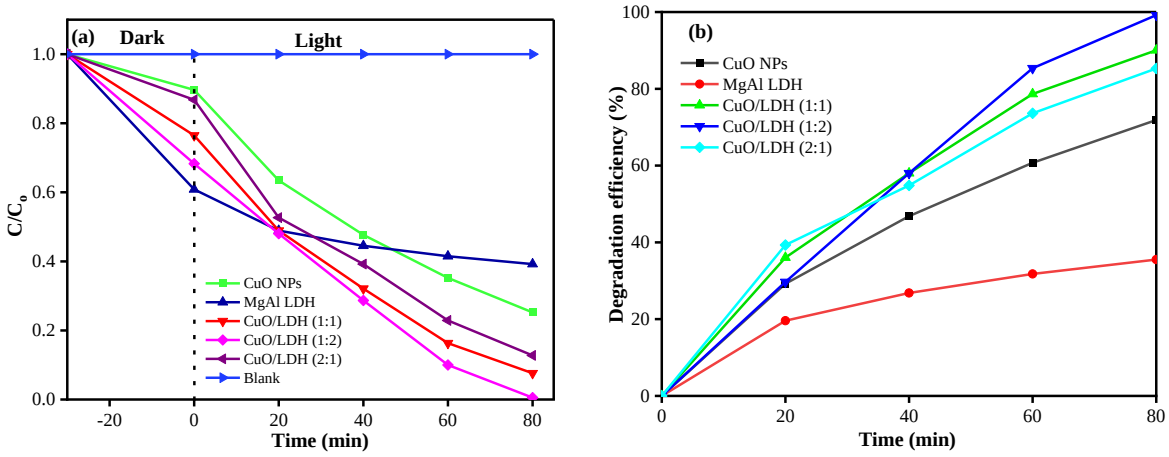

Fig. 16. Comparative examinations of the photocatalytic activity of the prepared materials when exposed to visible light.

4.8.1. Reaction Kinetics

As shown in Fig. 17, the performance of the samples in the photodegradation process was found to be consistent with the pseudo-first order reaction kinetics (Fu et al., 2019) after fitting the correlation data:

$$\ln\left(\frac{C}{Co}\right) = -Kt \qquad (6)$$

where C_0 is the MB concentration at time t=0 (when the light is turned on after the dark period), C is the MB concentration at photocatalytic reaction time t, and k is the decolorization

rate constant (min^{-1}). Table 4 provides detailed information on the kinetic parameters of the pseudo first-order fitting for methylene blue degradation. Under visible light, the degradation rate constant k for CuO/MgAl-LDH (1:2) was estimated to be 0.03141min^{-1}; this value was higher than that of pure CuO and all other samples, which fit well into the pseudo first-order kinetic model with correlation coefficients (R^2) equal to 0.90697. The findings showed that the CuO/MgAl-LDH composites have good photocatalytic activity when exposed to visible light (Zhao et al., 2018).

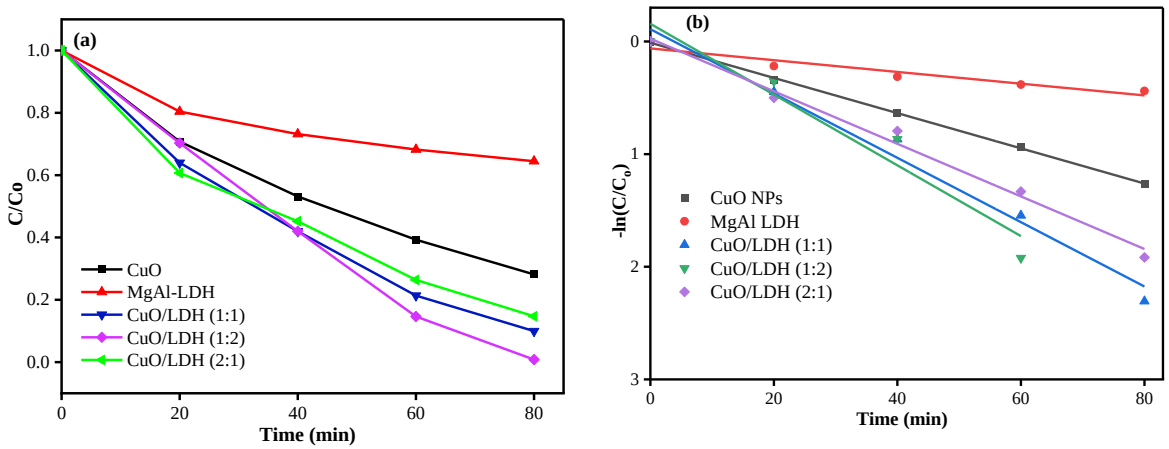

Fig. 17. Linear correlation between time and corresponding $\ln(C/Co)$ represented pseudo first order reaction between dye and photocatalysts.

Table 4: Parameters of the pseudo first-order kinetic model for photocatalytic degradation of methylene blue

Samples	K (min^{-1})	R^2
1:1 CuO NPs/MgAl LDH	0.02855	0.97584
1:2 CuO NPs/MgAl LDH	0.03141	0.90697
2:1 CuO NPs/MgAl LDH	0.02334	0.98519
CuO NPs	0.01563	0.9988
MgAl LDH	0.00521	0.9000

4.9. Reusability

The stability and reusability of the CuO NPs/MgAl-LDH (1:2) photocatalyst is an important property for real-time practical use (Zhu et al., 2016). CuO/MgAl-LDH (1:2) was repeatedly used for five cycles to further evaluate its cyclic performance within 80 minutes. The catalyst after each cycle was recovered by centrifugation, washed with deionized water, and dried in oven at 80 °C. There was no significant decrease in photocatalytic activity after recycling five times, and the slightly reduced activity is primarily due to mass loss of photocatalyst during centrifugation to collect the used catalyst for reuse as revealed in Fig. 18. Rather, the photocatalytic activity of CuO/MgAl-LDH (1:2) composites retained 92.7 % of its original activity, indicating that the prepared CuO/MgAl-LDH (1:2) composites had outstanding reusability and stability, as well as potential practical application value in environmental purification.

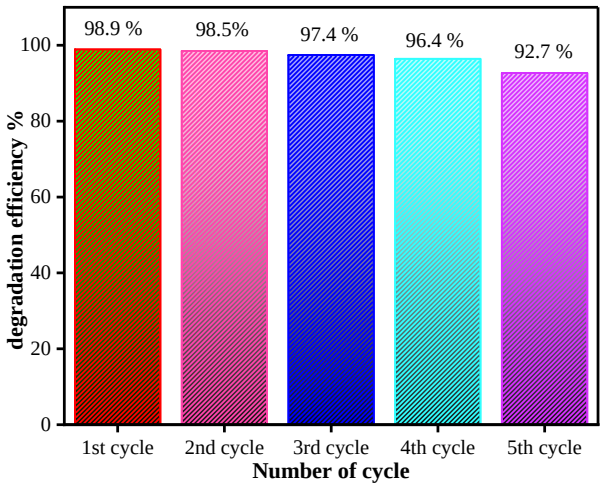

Fig. 18. Cyclic stability of CuO/MgAl-LDH (1:2) photocatalyst in degradation of MB dye under visible irradiation.

4.10. Proposed Photocatalytic Mechanism

The following photocatalytic degradation mechanism was proposed based on the results provided via the characterization techniques and photocatalytic experiments. First, a photon with energy equal to or greater than the bandgap energy strikes the surface of the CuO/MgAl LDH (1:2) nanocomposites. Whenever a photon hits an electron in the valence band, it absorbs its energy and jumps to the higher-energy conduction band. Such a process is called excitation

(A. George et al., 2022). CuO created electron-hole pairs when exposed to visible light (Khan et al., 2020). Then positive charges on the surface of LDHs platelets can attract electrons (e^-) produced by the CuO particles, while the holes (h^+) move to the opposite direction, leading to the separation of the photogenerated electron (e^-) - hole (h^+) pairs (L. Wang et al., 2019). The photogenerated holes (h^+) reacted with the water molecules adsorbed on the surface of the photocatalysts or with hydroxyl ions to produce hydroxyl radicals ($^{\bullet}OH$), and the $^{\bullet}OH$ radicals can then oxidize the organic contaminants (Zhao et al., 2018). Furthermore, the LDH layer's surface ^-OH groups react with valence band holes to produce hydroxyl radicals ($^{\bullet}OH$) with a high oxidation potential, which are significant variables in photo-oxidation reactions (Y. Wang et al., 2018). Simultaneously, Superoxide radicals ($^{\bullet}O_2^-$) were formed when excited electrons were caught by dissolved oxygen species in an aqueous solution (A. George et al., 2022). Organic matter was decomposed into inorganic small molecules like CO_2 and H_2O by reactive $^{\bullet}O_2^-$ and $^{\bullet}OH$ species with high activity (Sapkota et al., 2020). The high surface area of CuO NPs, which is effectively distributed over the LDH surface, and their synergistic impact in quick dye adsorption on LDH followed by rapid photodegradation by supported CuO NPs are attributable to the improved activity of CuO/MgAl-LDH (1:2) nanocomposites. The CuO is principally responsible for the increased efficiency of the photocatalytic activity of MB dye degradation. It should be highlighted that the strong interaction with LDH aided charge transport and improved the photocatalytic function of composites. Furthermore, the particle size of CuO was lowered to expose more active sites, and the contact area with the target pollutants was increased, both of which improved photocatalytic efficiency. LDH's adsorption capacity can bring organic pollutant molecules close to the catalyst surface, where hydroxyl and superoxide radicals are formed. Because the life of hydroxyl and superoxide radicals is only a few nanoseconds, they should react soon after formation. As a result, when pollutants bind to the LDH support, the produced radicals react with the pollutants molecules right away, before they may participate in side reactions or deactivation. The photoreaction's possible process is depicted schematically in Fig. 19. The details are as follows Equations.

$$\text{CuO/MgAl LDH} + h\nu \longrightarrow e^-_{(CB)} + h^+_{(VB)} \quad (7)$$

$$h^+_{(VB)} + H_2O\ (\text{adsorbed}) \longrightarrow \cdot OH + H^+ \quad (8)$$

$$h^+_{(VB)} + {}^-OH \longrightarrow \cdot OH \quad (9)$$

$$h^+_{(VB)} + MB* \longrightarrow \text{methylene blue} \quad (10)$$

$^{\cdot}OH + *\text{methylene blue} \longrightarrow \text{degradation products}$ (11)

$e^{-}_{(CB)} + O_2 \longrightarrow {}^{\cdot}O_2^{-}$ (12)

${}^{\cdot}O_2^{-} + H^{+} \longrightarrow HO_2^{\cdot}\ (HOO^{\cdot})$ (13)

${}^{\cdot}O_2^{-} + MB \longrightarrow \text{methylene blue-}OO^{\cdot}$ (14)

${}^{\cdot}O_2^{-} + HO_2^{\cdot} + H^{+} \longrightarrow H_2O_2 + O_2$ (15)

$e^{-}_{(CB)} + H_2O_2 \longrightarrow {}^{\cdot}OH$ (16)

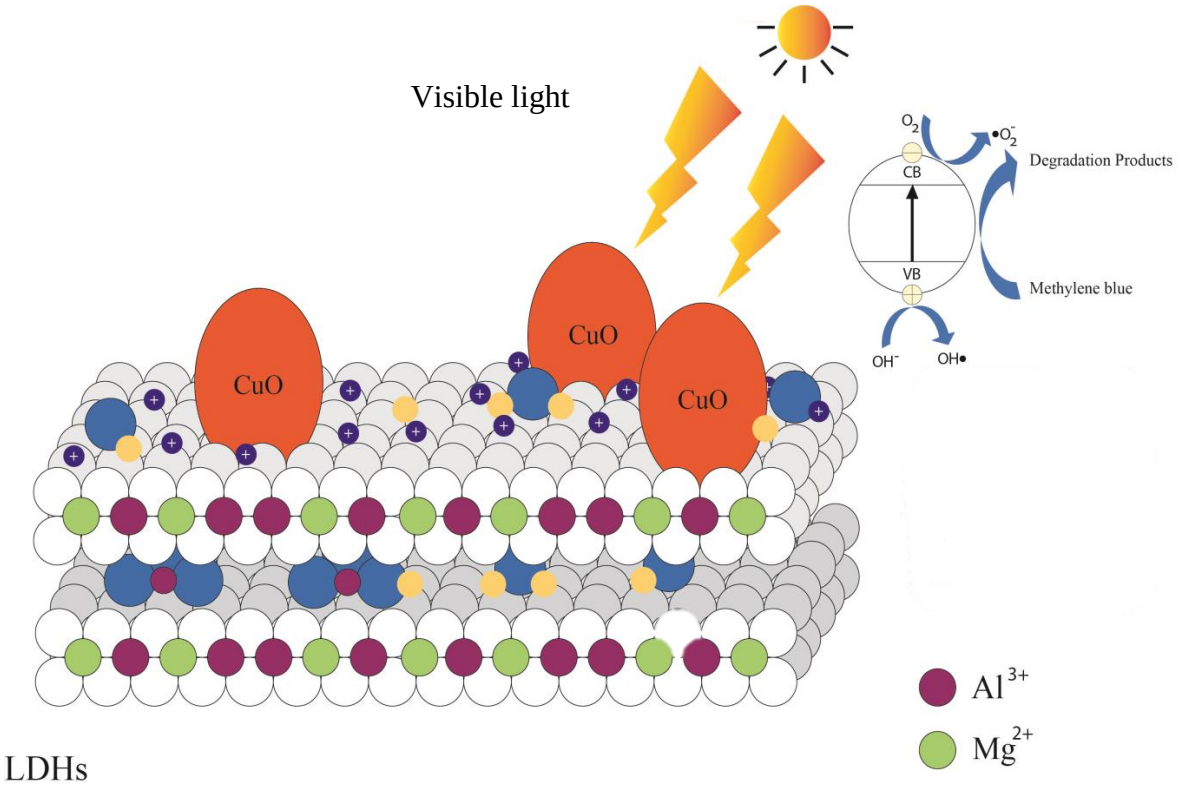

Fig. 19. The proposed mechanism of photocatalytic degradation of methylene blue.

CONCLUSION

This work describes a green method for producing CuO nanoparticles that use abundant, environmentally friendly *Allium cepa L*. peel extract which acted as reducing/capping agents. Moreover, MgAl-LDHs, and CuO/MgAl-LDH nanocomposites with varying the weight ratio (1:1, 1:2, and 2:1) were prepared by co-precipitation technique. XRD analysis approved the formation of pure monoclinic crystallite structures of CuO NPs, and well-organized two dimensional MgAl-LDHs. FTIR spectra confirm the synthesis of these nanocomposites. XPS survey scan confirmed the presence of Cu, Mg, Al, and O elements, which is consistent with the EDS data. SEM images show the spherical structure of CuO NPs was uniformly loaded on the surface of MgAl-LDHs. These observations were confirmed by TEM. UV-Vis DRS showed that the synthesized samples had efficiency of absorption in visible region. The CuO/MgAl-LDH (1:2) composite exhibit good photoluminescence property by extending the lifetime of photogenerated charge carriers and they also demonstrated a photocatalytic degradation efficiency of 99.20 % in 80 min for MB under visible light irradiation. However, only 90.03, 85.30, 71.87, and 35.53 % of MB dye are degraded by CuO/MgAl-LDH (1:1), CuO/MgAl-LDH (2:1), CuO, and MgAl-LDH catalysts, respectively. The enhanced photocatalytic activity was attributed to synergistic effect of the homogeneous dispersion of CuO NPs, adsorption of MB on MgAl-LDH, MgAl-hydroxyl-rich LDH's structure and lower band gap of CuO NPs. The kinetics of adsorption was all governed by a pseudo-first-order kinetic equation. After five recycle runs, it was revealed that about 92.7 % of the MB dye removal could still be maintained. This outstanding performance demonstrated the synthesized CuO/MgAl-LDH photocatalyst's potential utility in the elimination of organic contaminants.

RECOMMENDATIONS

The following suggestions are based on the work completed throughout this thesis and the previously stated conclusions:-

- We guide you to work with the Brunauer-Emmett-Teller (BET), which is used to compute the specific surface area of the samples.
- We propose that Electrochemical Impedance Spectroscopy (EIS) and Mott-Schotkky analyses be used to demonstrate the electron transport process and the flat band potential of semiconductors in detail. The latter method identifies whether the generated interface is a p-n or a Schottky junction.
- Furthermore, free radical scavenging tests should be performed to better understand the major active chemicals involved in the degradation reaction

REFERENCES

Abhilash, M. R., Akshatha, G., & Srikantaswamy, S. (2019). Photocatalytic dye degradation and biological activities of the Fe 2 O 3/Cu 2 O nanocomposite. *RSC advances*, *9*(15), 8557-8568.

Alsamhary, K., Al-Enazi, N. M., Alhomaidi, E., & Alwakeel, S. (2022). Spirulina platensis mediated biosynthesis of Cuo Nps and photocatalytic degradation of toxic azo dye Congo red and kinetic studies. *Environmental research*, *207*, 112172.

Aminuzzaman, M., Kei, L. M., & Liang, W. H. (2017). *Green synthesis of copper oxide (CuO) nanoparticles using banana peel extract and their photocatalytic activities.* Paper presented at the AIP Conference Proceedings.

Arora, N., Mehta, A., Mishra, A., & Basu, S. (2018). 4-Nitrophenol reduction catalysed by Au-Ag bimetallic nanoparticles supported on LDH: Homogeneous vs. heterogeneous catalysis. *Applied Clay Science*, *151*, 1-9.

Arunkumar, B., Jeyakumar, S. J., & Jothibas, M. (2019). A sol-gel approach to the synthesis of CuO nanoparticles using Lantana camara leaf extract and their photo catalytic activity. *Optik*, *183*, 698-705.

Asano, T., & Levine, A. D. (1996). Wastewater reclamation, recycling and reuse: past, present, and future. *Water science and technology*, *33*(10-11), 1-14.

Asemani, M., & Anarjan, N. (2019). Green synthesis of copper oxide nanoparticles using Juglans regia leaf extract and assessment of their physico-chemical and biological properties. *Green processing and synthesis*, *8*(1), 557-567.

Bekru, A. G., Zelekew, O. A., Andoshe, D. M., Sabir, F. K., & Eswaramoorthy, R. (2021). Microwave-Assisted Synthesis of CuO Nanoparticles Using Cordia africana Lam. Leaf Extract for 4-Nitrophenol Reduction. *Journal of Nanotechnology*, *2021*.

Bhaduri, A., & Kajal. (2019). *Facile synthesis and characterization of cupric oxide (CuO) nanoparticles: Inexpensive and abundant candidate for light harvesting.* Paper presented at the AIP Conference Proceedings.

Bhuvaneswari, K., Palanisamy, G., Pazhanivel, T., Bharathi, G., & Nataraj, D. (2018). Photocatalytic Performance on Visible Light Induced ZnS QDs-MgAl Layered Double Hydroxides Hybrids for Methylene Blue Dye Degradation. *ChemistrySelect*, *3*(47), 13419-13426.

Bilal Tahir, M., Nadeem Riaz, K., & Asiri, A. M. (2019). Boosting the performance of visible light-driven WO3/g-C3N4 anchored with BiVO4 nanoparticles for photocatalytic hydrogen evolution. *International Journal of Energy Research*, *43*(11), 5747-5758.

Bordbar, M., Sharifi-Zarchi, Z., & Khodadadi, B. (2017). Green synthesis of copper oxide nanoparticles/clinoptilolite using Rheum palmatum L. root extract: high catalytic activity for reduction of 4-nitro phenol, rhodamine B, and methylene blue. *Journal of sol-Gel science and Technology*, *81*(3), 724-733.

Buazar, F., Sweidi, S., Badri, M., & Kroushawi, F. (2019). Biofabrication of highly pure copper oxide nanoparticles using wheat seed extract and their catalytic activity: A mechanistic approach. *Green processing and synthesis*, *8*(1), 691-702.

Canbaz, G. T., Açikel, Ü., & Açikel, Y. S. Green Synthesis of ZnO Nanoparticles from Onion Peel Wastes.

Carja, G., Dartu, L., Okada, K., & Fortunato, E. (2013). Nanoparticles of copper oxide on layered double hydroxides and the derived solid solutions as wide spectrum active nano-photocatalysts. *Chemical Engineering Journal*, *222*, 60-66.

Chakraborty, S., Sarkar, I., Haldar, K., Pal, S. K., & Chakraborty, S. (2015). Synthesis of Cu–Al layered double hydroxide nanofluid and characterization of its thermal properties. *Applied Clay Science*, *107*, 98-108.

Chang, Z., Wu, C., Song, S., Kuang, Y., Lei, X., Wang, L., & Sun, X. (2013). Synthesis mechanism study of layered double hydroxides based on nanoseparation. *Inorganic chemistry, 52*(15), 8694-8698.

Chen, J., Wang, C., Zhang, Y., Guo, Z., Luo, Y., & Mao, C.-J. (2020). Engineering ultrafine NiS cocatalysts as active sites to boost photocatalytic hydrogen production of MgAl layered double hydroxide. *Applied Surface Science, 506*, 144999.

Chen, P., Chen, L., Dong, X. a., Wang, H., Li, J., Zhou, Y., . . . Dong, F. (2020). Enhanced Photocatalytic VOCs Mineralization via Special Ga-OH Charge Transfer Channel in α-Ga2O3/MgAl-LDH Heterojunction. *ACS ES&T Engineering, 1*(3), 501-511.

Chia, P. W., Lim, B. S., Tan, K. C., Yong, F. S. J., & Kan, S.-Y. (2019). Water extract of onion peel for the synthesis of bisindolylmethanes. *Journal of King Saud University-Science, 31*(4), 642-647.

Chia, P. W., Lim, B. S., Yong, F. S. J., Poh, S.-C., & Kan, S.-Y. (2018). An efficient synthesis of bisenols in water extract of waste onion peel ash. *Environmental Chemistry Letters, 16*(4), 1493-1499.

Choi, J., Oh, H., Han, S.-W., Ahn, S., Noh, J., & Park, J. B. (2017). Preparation and characterization of graphene oxide supported Cu, Cu2O, and CuO nanocomposites and their high photocatalytic activity for organic dye molecule. *Current Applied Physics, 17*(2), 137-145.

Chowdhury, R., Khan, A., & Rashid, M. H. (2020). Green synthesis of CuO nanoparticles using Lantana camara flower extract and their potential catalytic activity towards the aza-Michael reaction. *RSC advances, 10*(24), 14374-14385.

Das, P., Ghosh, S., Ghosh, R., Dam, S., & Baskey, M. (2018). Madhuca longifolia plant mediated green synthesis of cupric oxide nanoparticles: a promising environmentally sustainable material for waste water treatment and efficient antibacterial agent. *Journal of Photochemistry and Photobiology B: Biology, 189*, 66-73.

Dasineh Khiavi, N., Katal, R., Kholghi Eshkalak, S., Masudy-Panah, S., Ramakrishna, S., & Jiangyong, H. (2019). Visible light driven heterojunction photocatalyst of CuO–Cu2O thin films for photocatalytic degradation of organic pollutants. *Nanomaterials, 9*(7), 1011.

Deka, P., Deka, R. C., & Bharali, P. (2014). In situ generated copper nanoparticle catalyzed reduction of 4-nitrophenol. *New Journal of Chemistry, 38*(4), 1789-1793.

Dumitru, R., Ianculescu, A., Păcurariu, C., Lupa, L., Pop, A., Vasile, B., . . . Manea, F. (2019). BiFeO3-synthesis, characterization and its photocatalytic activity towards doxorubicin degradation from water. *Ceramics international, 45*(2), 2789-2802.

Dvininov, E., Ignat, M., Barvinschi, P., Smithers, M., & Popovici, E. (2010). New SnO2/MgAl-layered double hydroxide composites as photocatalysts for cationic dyes bleaching. *Journal of hazardous materials, 177*(1-3), 150-158.

Filiz, B. C. (2020). The role of catalyst support on activity of copper oxide nanoparticles for reduction of 4-nitrophenol. *Advanced Powder Technology, 31*(9), 3845-3859.

Fu, S., Zheng, Y., Zhou, X., Ni, Z., & Xia, S. (2019). Visible light promoted degradation of gaseous volatile organic compounds catalyzed by Au supported layered double hydroxides: influencing factors, kinetics and mechanism. *Journal of hazardous materials, 363*, 41-54.

Ganesan, K., Jothi, V. K., Natarajan, A., Rajaram, A., Ravichandran, S., & Ramalingam, S. (2020). Green synthesis of Copper oxide nanoparticles decorated with graphene oxide for anticancer activity and catalytic applications. *Arabian Journal of Chemistry, 13*(8), 6802-6814.

George, A., Raj, D. M. A., Venci, X., Raj, A. D., Irudayaraj, A. A., Josephine, R., . . . Chen, T.-W. (2022). Photocatalytic effect of CuO nanoparticles flower-like 3D nanostructures under visible light irradiation with the degradation of methylene blue (MB) dye for environmental application. *Environmental research, 203*, 111880.

George, G., & Saravanakumar, M. (2017). *Synthesising methods of layered double hydroxides and its use in the fabrication of dye Sensitised solar cell (DSSC): A short review.* Paper presented at the IOP Conference Series: Materials Science and Engineering.

Ghorai, T. K. (2015). Synthesis of spherical mesoporous titania modified iron-niobate nanoclusters for photocatalytic reduction of 4-nitrophenol. *Journal of Materials Research and Technology, 4*(2), 133-143.

Goel, S., Chen, F., & Cai, W. (2014). Synthesis and biomedical applications of copper sulfide nanoparticles: from sensors to theranostics. *Small, 10*(4), 631-645.

Gu, H., Chen, X., Chen, F., Zhou, X., & Parsaee, Z. (2018). Ultrasound-assisted biosynthesis of CuO-NPs using brown alga Cystoseira trinodis: Characterization, photocatalytic AOP, DPPH scavenging and antibacterial investigations. *Ultrasonics Sonochemistry, 41*, 109-119.

Hossain, S. S., Tarek, M., Munusamy, T. D., Karim, K. M. R., Roopan, S. M., Sarkar, S. M., . . . Khan, M. M. R. (2020). Facile synthesis of CuO/CdS heterostructure photocatalyst for the effective degradation of dye under visible light. *Environmental research, 188*, 109803.

Huang, G., Chen, J., Wang, D., Sun, Y., Jiang, L., Yu, Y., . . . Kang, Y. (2016). Nb2O5/ZnAl–LDH composites and its calcined products for photocatalytic degradation of congo red under visible light irradiation. *Materials Letters, 173*, 227-230.

Ifesan, B. O. (2017). Chemical composition of onion peel (Allium cepa) and its ability to serve as a preservative in cooked beef. *Int. J. Sci. Res. Methodol, 7*(4), 1-10.

Islam, M. R., Saiduzzaman, M., Nishat, S. S., Kabir, A., & Farhad, S. (2021). Synthesis, characterization and visible light-responsive photocatalysis properties of Ce doped CuO nanoparticles: A combined experimental and DFT+ U study. *Colloids and Surfaces A: Physicochemical and Engineering Aspects, 617*, 126386.

Jawad, A., Lu, X., Chen, Z., & Yin, G. (2014). Degradation of chlorophenols by supported Co–Mg–Al layered double hydrotalcite with bicarbonate activated hydrogen peroxide. *The Journal of Physical Chemistry A, 118*(43), 10028-10035.

Jiang, Z., Yan, L., Wu, J., Liu, X., Zhang, J., Zheng, Y., & Pei, Y. (2020). Low-temperature synthesis of carbonate-intercalated NixFe-layered double hydroxides for enhanced adsorption properties. *Applied Surface Science, 531*, 147281.

Kannan, K., Radhika, D., Vijayalakshmi, S., Sadasivuni, K. K., A. Ojiaku, A., & Verma, U. (2022). Facile fabrication of CuO nanoparticles via microwave-assisted method: photocatalytic, antimicrobial and anticancer enhancing performance. *International Journal of Environmental Analytical Chemistry, 102*(5), 1095-1108.

Keabadile, O. P., Aremu, A. O., Elugoke, S. E., & Fayemi, O. E. (2020). Green and traditional synthesis of copper oxide nanoparticles—comparative study. *Nanomaterials, 10*(12), 2502.

Kerchich, S., Boudjemaa, A., Chebout, R., Bachari, K., & Mameri, N. (2021). High performance of δ-Fe2O3 novel photo-catalyst supported on LDH structure. *Journal of Photochemistry and Photobiology A: Chemistry, 406*, 113001.

Khan, I., Khan, I., Usman, M., Imran, M., & Saeed, K. (2020). Nanoclay-mediated photocatalytic activity enhancement of copper oxide nanoparticles for enhanced methyl orange photodegradation. *Journal of Materials Science: Materials in Electronics, 31*(11), 8971-8985.

Kim, J., Kim, J.-S., & Park, E. (2013). Cytotoxic and anti-inflammatory effects of onion peel extract on lipopolysaccharide stimulated human colon carcinoma cells. *Food and chemical toxicology, 62*, 199-204.

Krishnasamy Sekar, R., Sridhar, A., Perumalsamy, B., Manikandan, D. B., & Ramasamy, T. (2020). In vitro antioxidant, antipathogenicity and cytotoxicity effect of silver nanoparticles fabricated by onion (Allium cepa L.) peel extract. *BioNanoScience, 10*(1), 235-248.

Kumar, V., Mohapatra, T., Dharmadhikari, S., & Ghosh, P. (2020). A review paper on heterogeneous Fenton catalyst: types of preparation, modification techniques, factors affecting the synthesis, characterization, and application in the wastewater treatment. *Bulletin of Chemical Reaction Engineering & Catalysis, 15*(1), 1-34.

Le Hoang, T. T. T., Insin, N., & Sukpirom, N. (2020). Catalytic activity of silver nanoparticles anchored on layered double hydroxides and hydroxyapatite. *Inorganic Chemistry Communications, 121*, 108199.

Lee, K. A., Kim, K.-T., Kim, H. J., Chung, M.-S., Chang, P.-S., Park, H., & Pai, H.-D. (2014). Antioxidant activities of onion (Allium cepa L.) peel extracts produced by ethanol, hot water, and subcritical water extraction. *Food Science and Biotechnology, 23*(2), 615-621.

Lem, O., Yoon, S., Bae, S., & Lee, W. (2021). The enhanced reduction of bromate by highly reactive and dispersive green nano-zerovalent iron (G-NZVI) synthesized with onion peel extract. *RSC advances, 11*(9), 5008-5018.

Li, F., & Duan, X. (2006). Applications of layered double hydroxides *Layered double hydroxides* (pp. 193-223): Springer.

Li, X., Xue, J., Ma, S., Xu, P., Huang, C., & Wang, M. (2019). Synthesis of MgAl LDH/Acidified g-C3N4 heterojunction photocatalyst for improved tetracycline hydrochloride degradation activity. *Nano, 14*(06), 1950066.

Li, Z., Chen, M., Ai, Z., Wu, L., & Zhang, Q. (2018). Mechanochemical synthesis of CdS/MgAl LDH-precursor as improved visible-light driven photocatalyst for organic dye. *Applied Clay Science, 163*, 265-272.

Lim, W. Y., & Ho, G. W. (2017). Nickel-Cobalt layered double hydroxides for photocatalytic degradation under visible light irradiation. *Procedia engineering, 215*, 163-170.

Liu, T., & Bai, X. (2021). In situ preparation of highly dispersed Pd supported on exfoliated layered double hydroxides via nitrogen plasma for 4-nitrophenol reduction. *Environmental Science and Pollution Research, 28*(23), 30090-30100.

Lucchesi Schio, A., Farias Soares, M. R., Machado, G., & Barcellos, T. (2021). Improved Mechanochemical Fabrication of Copper (II) Oxide Nanoparticles with Low E-Factor. Efficient Catalytic Activity for Nitroarene Reduction in Aqueous Medium. *ACS Sustainable Chemistry & Engineering, 9*(29), 9661-9670.

Ma, J., Ding, J., Li, L., Zou, J., Kong, Y., & Komarneni, S. (2015). In situ reduction for synthesis of nano-sized Cu2O particles on MgCuAl-LDH layers for degradation of orange II under visible light. *Ceramics international, 41*(2), 3191-3196.

Madima, N., Mishra, S., Inamuddin, I., & Mishra, A. (2020). Carbon-based nanomaterials for remediation of organic and inorganic pollutants from wastewater. A review. *Environmental Chemistry Letters, 18*(4), 1169-1191.

Mahmoud, R., Moaty, S. A., Mohamed, F., & Farghali, A. (2017). Comparative study of single and multiple pollutants system using Ti–Fe chitosan LDH adsorbent with high performance in wastewater treatment. *Journal of Chemical & Engineering Data, 62*(11), 3703-3722.

Malak-Polaczyk, A., Vix-Guterl, C., & Frackowiak, E. (2010). Carbon/layered double hydroxide (LDH) composites for supercapacitor application. *Energy & fuels, 24*(6), 3346-3351.

Mandlimath, T. R., & Gopal, B. (2011). Catalytic activity of first row transition metal oxides in the conversion of p-nitrophenol to p-aminophenol. *Journal of Molecular Catalysis A: Chemical, 350*(1-2), 9-15.

Manjari, G., Saran, S., Arun, T., Rao, A. V. B., & Devipriya, S. P. (2017). Catalytic and recyclability properties of phytogenic copper oxide nanoparticles derived from Aglaia elaeagnoidea flower extract. *Journal of Saudi Chemical Society, 21*(5), 610-618.

Masudy-Panah, S., Zhuk, S., Tan, H. R., Gong, X., & Dalapati, G. K. (2018). Palladium nanostructure incorporated cupric oxide thin film with strong optical absorption, compatible charge collection and low recombination loss for low cost solar cell applications. *Nano Energy, 46*, 158-167.

Morimoto, K., Tamura, K., Iyi, N., Ye, J., & Yamada, H. (2011). Adsorption and photodegradation properties of anionic dyes by layered double hydroxides. *Journal of Physics and Chemistry of Solids, 72*(9), 1037-1045.

Mousa, M. K. H. (2013). *Wastewater disinfection by synthesized copper oxide nanoparticles stabilized with surfactant.*

Moustafa, D., Mahmoud, R., El-Salam, H. M. A., & Shehata, N. (2021). Utilization of residual zinc–iron-layered double hydroxide after methyl orange management as a new sorbent for wastewater treatment. *Applied Nanoscience, 11*(2), 709-723.

Musyoka, N. M., Mutuma, B. K., & Manyala, N. (2020). Onion-derived activated carbons with enhanced surface area for improved hydrogen storage and electrochemical energy application. *RSC advances, 10*(45), 26928-26936.

Muthuvel, A., Jothibas, M., & Manoharan, C. (2020). Synthesis of copper oxide nanoparticles by chemical and biogenic methods: photocatalytic degradation and in vitro antioxidant activity. *Nanotechnology for Environmental Engineering, 5*(2), 1-19.

Nasrollahzadeh, M., Maham, M., & Sajadi, S. M. (2015). Green synthesis of CuO nanoparticles by aqueous extract of Gundelia tournefortii and evaluation of their catalytic activity for the synthesis of N-monosubstituted ureas and reduction of 4-nitrophenol. *Journal of colloid and interface science, 455*, 245-253.

Nayak, S., & Parida, K. (2016). Nanostructured CeO2/MgAl-LDH composite for visible light induced water reduction reaction. *International Journal of Hydrogen Energy, 41*(46), 21166-21180.

Ni, J., Xue, J., Xie, L., Shen, J., He, G., & Chen, H. (2018). Construction of magnetically separable NiAl LDH/Fe 3 O 4–RGO nanocomposites with enhanced photocatalytic performance under visible light. *Physical Chemistry Chemical Physics, 20*(1), 414-421.

Nordin, N. R., & Shamsuddin, M. (2019). Biosynthesis of copper (II) oxide nanoparticles using Murayya koeniggi aqueous leaf extract and its catalytic activity in 4-nitrophenol reduction. *Malaysian Journal of Fundamental and Applied Sciences, 15*, 218-224.

Palapa, N. R., Taher, T., Rahayu, B. R., Mohadi, R., Rachmat, A., & Lesbani, A. (2020). CuAl LDH/Rice Husk Biochar Composite for Enhanced Adsorptive Removal of Cationic Dye from Aqueous Solution. *Bulletin of Chemical Reaction Engineering & Catalysis*, *15*(2).

Patel, M., Mishra, S., Verma, R., & Shikha, D. (2022). Synthesis of ZnO and CuO nanoparticles via Sol gel method and its characterization by using various technique. *Discover Materials*, *2*(1), 1-11.

Patra, J. K., & Baek, K.-H. (2015). Novel green synthesis of gold nanoparticles using Citrullus lanatus rind and investigation of proteasome inhibitory activity, antibacterial, and antioxidant potential. *International journal of nanomedicine, 10*, 7253.

Patra, J. K., Kwon, Y., & Baek, K.-H. (2016). Green biosynthesis of gold nanoparticles by onion peel extract: Synthesis, characterization and biological activities. *Advanced Powder Technology, 27*(5), 2204-2213.

Rafique, M., Shafiq, F., Gillani, S. S. A., Shakil, M., Tahir, M. B., & Sadaf, I. (2020). Eco-friendly green and biosynthesis of copper oxide nanoparticles using Citrofortunella microcarpa leaves extract for efficient photocatalytic degradation of Rhodamin B dye form textile wastewater. *Optik, 208*, 164053.

Rafique, M., Shaikh, A. J., Rasheed, R., Tahir, M. B., Gillani, S. S. A., Usman, A., . . . Rabbani, F. (2018). Aquatic biodegradation of methylene blue by copper oxide nanoparticles synthesized from Azadirachta indica leaves extract. *Journal of Inorganic and Organometallic Polymers and Materials, 28*(6), 2455-2462.

Rafique, M. A., Kiran, S., Javed, S., Ahmad, I., Yousaf, S., Iqbal, N., . . . Rani, F. (2021). Green synthesis of nickel oxide nanoparticles using Allium cepa peels for degradation of Congo red direct dye: an environmental remedial approach. *Water science and technology, 84*(10-11), 2793-2804.

Rani Verma, P., & Khan, F. (2019). Green approach for biofabrication of CuO nanoparticles from Prunus amygdalus pericarp extract and characterization. *Inorganic and Nano-Metal Chemistry, 49*(3), 69-74.

Rao, M. P., Sathishkumar, P., Mangalaraja, R. V., Asiri, A. M., Sivashanmugam, P., & Anandan, S. (2018). Simple and low-cost synthesis of CuO nanosheets for visible-light-driven

photocatalytic degradation of textile dyes. *Journal of Environmental Chemical Engineering, 6*(2), 2003-2010.

Rao, M. P., Wu, J. J., Asiri, A. M., Anandan, S., & Ashokkumar, M. (2018). Photocatalytic properties of hierarchical CuO nanosheets synthesized by a solution phase method. *Journal of Environmental Sciences, 69*, 115-124.

Rijsberman, F. R. (2006). Water scarcity: fact or fiction? *Agricultural water management, 80*(1-3), 5-22.

Sakib, A. A. M., Masum, S. M., Hoinkis, J., Islam, R., Molla, M., & Islam, A. (2019). Synthesis of CuO/ZnO nanocomposites and their application in photodegradation of toxic textile dye. *Journal of Composites Science, 3*(3), 91.

Sanakousar, F., Vidyasagar, C., Jiménez-Pérez, V., & Prakash, K. (2022). Recent progress on visible-light-driven metal and non-metal doped ZnO nanostructures for photocatalytic degradation of organic pollutants. *Materials Science in Semiconductor Processing, 140*, 106390.

Sangkhum, P., Yanamphorn, J., Wangriya, A., & Ngamcharussrivichai, C. (2019). Ca–Mg–Al ternary mixed oxides derived from layered double hydroxide for selective etherification of glycerol to short-chain polyglycerols. *Applied Clay Science, 173*, 79-87.

Sapkota, K. P., Lee, I., Hanif, M., Islam, M., Akter, J., & Hahn, J. R. (2020). Enhanced visible-light photocatalysis of nanocomposites of copper oxide and single-walled carbon nanotubes for the degradation of methylene blue. *Catalysts, 10*(3), 297.

Sarkar, C., & Dolui, S. K. (2015). Synthesis of copper oxide/reduced graphene oxide nanocomposite and its enhanced catalytic activity towards reduction of 4-nitrophenol. *RSC advances, 5*(75), 60763-60769.

Sathiyavimal, S., Vasantharaj, S., Veeramani, V., Saravanan, M., Rajalakshmi, G., Kaliannan, T., . . . Pugazhendhi, A. (2021). Green chemistry route of biosynthesized copper oxide nanoparticles using Psidium guajava leaf extract and their antibacterial activity and effective removal of industrial dyes. *Journal of Environmental Chemical Engineering, 9*(2), 105033.

Scarpellini, D., Falconi, C., Gaudio, P., Mattoccia, A., Medaglia, P., Orsini, A., . . . Richetta, M. (2014). Morphology of Zn/Al layered double hydroxide nanosheets grown onto aluminum thin films. *Microelectronic Engineering, 126*, 129-133.

Seftel, E., Mertens, M., & Cool, P. (2013). The influence of the Ti4+ location on the formation of self-assembled nanocomposite systems based on TiO2 and Mg/Al-LDHs with photocatalytic properties. *Applied Catalysis B: Environmental, 134*, 274-285.

Seftel, E., Popovici, E., Beyers, E., Mertens, M., Zhu, H., Vansant, E., & Cool, P. (2010). New TiO2/MgAl-LDH nanocomposites for the photocatalytic degradation of dyes. *Journal of nanoscience and nanotechnology, 10*(12), 8227-8233.

Senobari, S., & Nezamzadeh-Ejhieh, A. (2018). A comprehensive study on the enhanced photocatalytic activity of CuO-NiO nanoparticles: designing the experiments. *Journal of Molecular Liquids, 261*, 208-217.

Shahabadi, N., Razlansari, M., Zhaleh, H., & Mansouri, K. (2019). Antiproliferative effects of new magnetic pH-responsive drug delivery system composed of Fe3O4, CaAl layered double hydroxide and levodopa on melanoma cancer cells. *Materials Science and Engineering: C, 101*, 472-486.

Shan, R.-r., Yan, L.-g., Yang, K., Yu, S.-j., Hao, Y.-f., Yu, H.-q., & Du, B. (2014). Magnetic Fe3O4/MgAl-LDH composite for effective removal of three red dyes from aqueous solution. *Chemical Engineering Journal, 252*, 38-46.

Sharmila, G., Thirumarimurugan, M., & Sivakumar, V. M. (2016). Optical, catalytic and antibacterial properties of phytofabricated CuO nanoparticles using Tecoma castanifolia leaf extract. *Optik, 127*(19), 7822-7828.

Singh, J., Kumar, V., Kim, K.-H., & Rawat, M. (2019). Biogenic synthesis of copper oxide nanoparticles using plant extract and its prodigious potential for photocatalytic degradation of dyes. *Environmental research, 177*, 108569.

Sobhana, L., Sarakha, M., Prevot, V., & Fardim, P. (2016). Layered double hydroxides decorated with Au-Pd nanoparticles to photodegradate Orange II from water. *Applied Clay Science, 134*, 120-127.

Soori, F., & Nezamzadeh-Ejhieh, A. (2018). Synergistic effects of copper oxide-zeolite nanoparticles composite on photocatalytic degradation of 2, 6-dimethylphenol aqueous solution. *Journal of Molecular Liquids, 255*, 250-256.

Sukumar, S., Rudrasenan, A., & Padmanabhan Nambiar, D. (2020). Green-synthesized rice-shaped copper oxide nanoparticles using Caesalpinia bonducella seed extract and their applications. *ACS omega*, *5*(2), 1040-1051.

Surendhiran, S., Gowthambabu, V., Balamurugan, A., Sudha, M., Kumar, V. S., & Suresh, K. (2021). Rapid green synthesis of CuO nanoparticles and evaluation of its photocatalytic and electrochemical corrosion inhibition performance. *Materials Today: Proceedings, 47*, 1011-1016.

Tang, Y., Wang, R., Yang, Y., Yan, D., & Xiang, X. (2016). Highly enhanced photoelectrochemical water oxidation efficiency based on triadic quantum dot/layered double hydroxide/BiVO4 photoanodes. *ACS applied materials & interfaces, 8*(30), 19446-19455.

Vaidehi, D., Bhuvaneshwari, V., Bharathi, D., & Sheetal, B. P. (2018). Antibacterial and photocatalytic activity of copper oxide nanoparticles synthesized using Solanum lycopersicum leaf extract. *Materials Research Express, 5*(8), 085403.

Valdez, R., Grotjahn, D. B., Smith, D. K., Quintana, J. M., & Olivas, A. (2015). Nanosheets of Co-(Ni and Fe) layered double hydroxides for electrocatalytic water oxidation reaction. *Int. J. Electrochem. Sci, 10*(1), 909-918.

Valente, J. S., Tzompantzi, F., & Prince, J. (2011). Highly efficient photocatalytic elimination of phenol and chlorinated phenols by CeO2/MgAl layered double hydroxides. *Applied Catalysis B: Environmental, 102*(1-2), 276-285.

Varnagiris, S., Urbonavicius, M., Sakalauskaite, S., Daugelavicius, R., Pranevicius, L., Lelis, M., & Milcius, D. (2020). Floating TiO2 photocatalyst for efficient inactivation of E. coli and decomposition of methylene blue solution. *Science of the Total Environment, 720*, 137600.

Veisi, H., Karmakar, B., Tamoradi, T., Hemmati, S., Hekmati, M., & Hamelian, M. (2021). Biosynthesis of CuO nanoparticles using aqueous extract of herbal tea (Stachys Lavandulifolia) flowers and evaluation of its catalytic activity. *Scientific Reports, 11*(1), 1-13.

Wang, L., Gao, X., Cheng, Y., Zhang, X., Wang, G., Zhang, Q., & Su, J. (2019). TiO2@ MgAl-layered double hydroxide with enhanced photocatalytic activity towards degradation of gaseous toluene. *Journal of Photochemistry and Photobiology A: Chemistry*, *369*, 44-53.

Wang, Q., & O'Hare, D. (2012). Recent advances in the synthesis and application of layered double hydroxide (LDH) nanosheets. *Chemical reviews, 112*(7), 4124-4155.

Wang, Y., Jing, Y., Li, W., Yu, M., Ao, X., Xie, Y., & Chen, Q. (2018). Silicate silver/flower-like magnalium hydroxide composites for enhanced visible light photodegradation activities. *RSC advances*, *8*(41), 23442-23450.

Wu, X., Zhang, D., Jiao, F., & Wang, S. (2016). Visible-light-driven photodegradation of Methyl Orange using Cu2O/ZnAl calcined layered double hydroxides as photocatalysts. *Colloids and Surfaces A: Physicochemical and Engineering Aspects, 508*, 110-116.

Wu, Y.-g., Wen, M., Wu, Q.-s., & Fang, H. (2014). Ni/graphene nanostructure and its electron-enhanced catalytic action for hydrogenation reaction of nitrophenol. *The Journal of Physical Chemistry C, 118*(12), 6307-6313.

Xue, X., Yu, F., Peng, B., Wang, G., Lv, Y., Chen, L., . . . Guo, X. (2019). One-step synthesis of nickel–iron layered double hydroxides with tungstate acid anions via flash nano-precipitation for the oxygen evolution reaction. *Sustainable energy & fuels, 3*(1), 237-244.

Yang, K., Yan, Y., Wang, H., Sun, Z., Chen, W., Kang, H., . . . Li, Z. (2018). Monodisperse Cu/Cu 2 O@ C core–shell nanocomposite supported on rGO layers as an efficient catalyst derived from a Cu-based MOF/GO structure. *Nanoscale*, *10*(37), 17647-17655.

Yuan, J., Zhang, J.-J., Yang, M.-P., Meng, W.-J., Wang, H., & Lu, J.-X. (2018). CuO nanoparticles supported on TiO2 with high efficiency for CO2 electrochemical reduction to ethanol. *Catalysts, 8*(4), 171.

Zaghloul, A., Benhiti, R., Soudani, A., Chiban, M., Zerbet, M., & Sinan, F. (2019). Removal of methyl orange from aqueous solution using synthetic clay type MgAl-LDH: Characterization, Isotherm and thermodynamic studies. *Mediterranean Journal of Chemistry, 9*(2), 155-163.

Zhang, J., Gao, S., Wang, G., Ma, X., Jiao, S., Sang, D., . . . Wang, J. (2019). Tunable fabrication of CuO nanoplates on ZnO nanorods: Heterostructure formation by photodeposition for enhanced photocatalytic activity. *European Journal of Inorganic Chemistry, 2019*(21), 2654-2660.

Zhang, Y., Wu, B., Xu, H., Liu, H., Wang, M., He, Y., & Pan, B. (2016). Nanomaterials-enabled water and wastewater treatment. *NanoImpact, 3*, 22-39.

Zhao, G., Zou, J., Li, C., Yu, J., Jiang, X., Zheng, Y., . . . Jiao, F. (2018). Enhanced photocatalytic degradation of rhodamine B, methylene blue and 4-nitrophenol under visible light irradiation using TiO2/MgZnAl layered double hydroxide. *Journal of Materials Science: Materials in Electronics, 29*(8), 7002-7014.

Zhen, S.-y., Wu, H.-t., Wang, Y., Li, N., Chen, H.-s., Song, W.-l., . . . Sun, K.-n. (2019). Metal–organic framework derived hollow porous CuO–CuCo 2 O 4 dodecahedrons as a cathode catalyst for Li–O 2 batteries. *RSC advances, 9*(29), 16288-16295.

Zheng, G., Wu, C., Wang, J., Mo, S., Wang, Y., Zou, Z., . . . Long, F. (2019). Facile synthesis of few-layer MoS 2 in MgAl-LDH layers for enhanced visible-light photocatalytic activity. *RSC advances, 9*(42), 24280-24290.

Zhi, Y., Li, Y., Zhang, Q., & Wang, H. (2010). ZnO nanoparticles immobilized on flaky layered double hydroxides as photocatalysts with enhanced adsorptivity for removal of acid red G. *Langmuir, 26*(19), 15546-15553.

Zhou, Y., Hu, W., Yu, J., & Jiao, F. (2015). Effective photocatalytic degradation of methylene blue by Cu2O/MgAl layered double hydroxides. *Reaction Kinetics, Mechanisms and Catalysis, 115*(2), 581-596.

Zhou, Z., Lu, C., Wu, X., & Zhang, X. (2013). Cellulose nanocrystals as a novel support for CuO nanoparticles catalysts: facile synthesis and their application to 4-nitrophenol reduction. *RSC advances, 3*(48), 26066-26073.

Zhu, C., Zheng, J., Fang, L., Hu, P., Liu, Y., Cao, X., & Wu, M. (2016). Advanced visible-light driven photocatalyst with enhanced charge separation fabricated by facile deposition of Ag3PO4 nanoparticles on graphene-like h-BN nanosheets. *Journal of Molecular Catalysis A: Chemical, 424*, 135-144.

Zubair, M., Daud, M., McKay, G., Shehzad, F., & Al-Harthi, M. A. (2017). Recent progress in layered double hydroxides (LDH)-containing hybrids as adsorbents for water remediation. *Applied Clay Science, 143*, 279-292.

Research Fund Acknowledgement

This research thesis was funded by Adama Science and Technology University under the grant number of ASTU/SM-R/608/22, Adama, Ethiopia.